AD-A268 884

1. [illegible]

3. REPORT TYPE AND DATES COVERED
Final Report 01 Sep 87 - 30 Apr 93

4. TITLE AND SUBTITLE
High resolution SQUID Magnetometry for Non-destructive Evaluation

5. FUNDING NUMBERS
AFOSR-87-0337

6. AUTHOR(S)
Professor John P. Wikswo

7. PERFORMING ORGANIZATION NAME(S) AND ADDRESS(ES)
Electromagnetic Laboratory
Department of Physics & Astronomy
Vanderbilt University
Box 1807 Station B,
Nashville, TN 37235

8. PERFORMING ORGANIZATION REPORT NUMBER
AFOSR-TR- 93 0659

9. SPONSORING/MONITORING AGENCY NAME(S) AND ADDRESS(ES)
AFOSR/NE
110 DUNCAN AVENUE SUITE B115
BOLLING AFB DC 20332-0001

HAROLD WEINSTOCK

10. SPONSORING/MONITORING AGENCY REPORT NUMBER
2305/GS

11. SUPPLEMENTARY NOTES

12a. DISTRIBUTION/AVAILABILITY STATEMENT
UNLIMITED

This document has been approved for public release and sale; its distribution is unlimited.

12b. DISTRIBUTION CODE

13. ABSTRACT (Maximum 200 words)

SEE REPORT FOR ABSTRACT

14. SUBJECT TERMS

15. NUMBER OF PAGES
27

16. PRICE CODE

17. SECURITY CLASSIFICATION OF REPORT	18. SECURITY CLASSIFICATION OF THIS PAGE	19. SECURITY CLASSIFICATION OF ABSTRACT	20. LIMITATION OF ABSTRACT
UNCLASS	UNCLASS	UNCLASS	UL

FINAL REPORT FOR GRANT AFOSR-87-0337

High resolution SQUID Magnetometry for Non-destructive Evaluation

John P. Wikswo, Jr., Principal Investigator

Electromagnetics Laboratory, Department of Physics and Astronomy
Vanderbilt University, Box 1807 Station B, Nashville, TN 37235

ABSTRACT

Superconducting QUantum Interference Device (SQUID) magnetometers offer promise as multi-mode instruments capable of obtaining high resolution images of extremely low frequency injected currents or eddy currents, and they can be configured to image the magnetic susceptibility of titanium, aluminum and nonmetallic composites. While high resolution SQUID magnetometers will generally be noisier than conventional SQUIDs, the small coils and reduced coil-to-source spacing more than compensate to provide low-noise, high-resolution images. The high spatial resolution which can be obtained with SQUID magnetometers, the unparalleled sensitivity of SQUIDs at low frequencies, the ability to measure weak perturbations in strong applied magnetic fields, and the ability to discriminate against external sources of noise should make SQUID magnetometers well suited for NDE of deep flaws in aluminum and titanium aerostructures. To explore SQUID NDE, we have developed research facilities that include the high-resolution MicroSQUID magnetometer, a magnetic shield, a scanning stage, and a computer-based control and data acquisition system. Using this instrumentation, we have imaged magnetic fields produced by sources as varied as intrinsic currents due to corrosion or Johnson noise, remanent magnetization from ferromagnetic contamination, flaw-induced perturbations in either injected current or eddy currents induced by an AC field, Johnson noise currents in a copper ring, persistent currents in high transition-temperature superconductors, distributions of dia- or paramagnetism in an AC or DC magnetic field, and surface flaws decorated with a paramagnetic tracer. In support of the experimental studies, we have developed analytical and numerical models for the simulation of flaws with several geometries inside thick and thin current-carrying plates and thin-walled tubes, and have demonstrated that two-dimensional magnetic images can be deconvolved into images of current or magnetization by filtering techniques, finite element models, lead field analyses, and maximum entropy methods. We find that potential applications of SQUID NDE to the aging aircraft problem include high resolution imaging of flaws and corrosion deep inside second and third layer structures and turbine rings, and magnetic susceptibility imaging of corrosion, nonmetallic composites and magnetically-decorated surface flaws in ceramics. However, a critical assessment of the capabilities of SQUID NDE will require developing quantitative measures of SQUID NDE, such as the probability of detection of various sizes and locations of flaws. As instruments built specifically for NDE become more advanced, and as experience is gained worldwide in SQUID NDE, specific applications will undoubtedly be found for which the capabilities of SQUIDs are unmatched; whether or not this is sufficient to lead to widespread utilization of SQUIDs for aircraft NDE will then be a matter of economics, ease of use, and perception by the user community.

1. INTRODUCTION

While SQUID magnetometry has been successfully applied to a broad spectrum of problems in physics, biology, engineering, and geology, there has been only limited use of SQUIDs for non-destructive evaluation. The first demonstrations were by Weinstock and Nisenoff[1] in 1985. Since then, SQUIDs have been used to examine or detect ferromagnetic plates[2,3,4,5], naval mines[6], and wrist watches[7]; as an amplifier to detect eddy current signals[8], for monitoring corrosion in buried gas pipes[9,10]; and for fundamental measurements on the Barkhausen effect[11,12]. The work on corrosion on pipes is now being performed using fluxgate magnetometers[13]. There have been only two SQUID NDE review articles[14,15]. The limited effort on SQUID NDE has occurred for several reasons: SQUID magnetometers typically have more sensitivity than is necessary for most NDE applications; SQUID pickup coils, ordinarily optimized for clinical biomedical measurements on humans, are too large and too far from the sample to provide the requisite spatial resolution to compete with state-of-the-art eddy current and ultrasound techniques; and few of the

research groups doing SQUID NDE have programs that simultaneously develop instrumentation and mathematical models while conducting experiments that push the understanding of both the magnetic fields and their measurement.

One of the unfortunate misperceptions of the NDE user community is that SQUID magnetometers are suitable only for laboratory analysis. In part, this error arises from the requirement of SQUID magnetometers for liquid helium. There are several notable examples that demonstrate the success of SQUIDs outside the laboratory. For many years, SQUID-based rock magnetometers have even been installed in deep sea drilling ships, and, through the use of a nitrogen-temperature cryocooler, have a liquid helium hold-time of almost a year[15]. A compact SQUID magnetometer system, recently available commercially, is capable of being operated at the end of a robot manipulator arm in a magnetically-harsh industrial environment[17]. A 70 gigahertz sampling oscilloscope with less than a one-minute cool down time has been sold commercially, and a prototype version has been produced using a closed-cycle refrigerator[18]. In fairness to the cryogenically inexperienced, the need to transfer liquid helium, its cost, and the logistical problems with securing delivery of liquid helium to remote sites have all contributed to the slow acceptance of SQUID-based devices outside the laboratory.

The discovery of high temperature superconductors with transition temperature above 100 K will change this situation completely. Steady progress has been made towards the fabrication of high temperature superconducting components and devices by a number of companies, including DuPont, Conductus, TRW, IBM, Biomagnetic Technologies, and American Superconductor, as well as several university laboratories and government agencies such as the National Institute of Standards and Technology. Several laboratories have produced DC SQUID devices with lower noise than helium-temperature RF SQUID magnetometers, and there are predictions that the high-frequency sensitivity of high-temperature SQUIDs will soon approach that of commercially-available low temperature SQUIDs. A high-T_c SQUID, Mr.SQUID™, is now available, as an off-the-shelf product, for educational use[19], and by year's-end a version of this device with complete feedback electronics may be available as a simple yet complete SQUID magnetometer system whose sensitivity will far exceed that of commercial fluxgate magnetometers. Thus in the course of the next several years, it is reasonable to assume that a spectrum of high-T_c SQUID magnetometer systems will be available commercially, if not on a production basis definitely on a custom-fabrication one.

The discovery of high-temperature superconductors has also initiated major, new research programs in cryogenic technology, since 100 K can be readily achieved with an inexpensive, portable refrigerator. It would not be surprising to find a SQUID magnetometer mounted on a miniature refrigerator within 3 to 4 years, or even sooner. While it is unlikely that high-T_c SQUIDs and their associated refrigerators will provide the absolute sensitivity presently afforded by the low-T_c SQUID systems being manufactured for magnetoencephalography, it should also be clear from the data presented in this paper that most SQUID NDE signals are vastly larger than biomagnetic ones. As an example of readily achieved sensitivity, a high-T_c SQUID with a 2 mm^2 area hole in the SQUID washer will have a flux noise of $10^{-4}\phi_o/\sqrt{Hz}$, which would translate to a field noise of 10^{-13} T/$\sqrt{Hz}$, equivalent to that presently achieved by the liquid helium-cooled MicroSQUID magnetometer in use at Vanderbilt[20].

The key concern, of course, is not only SQUID noise, but environmental noise. In the past several years, there have been some noteworthy accomplishments in gradiometer design and active noise cancellation. Because the flaws being examined in flight-line NDE of aircraft would be at most several centimeters beneath the outer surface, gradiometer baselines can be of comparable dimension, which is substantially shorter than that used in many biomedical systems. The addition of reference magnetometer channels to sense ambient noise and the use of computer-controlled AC cancellation of drive current crosstalk has made it possible to operate SQUID NDE systems in a particularly-hostile industrial environment[17]. In the case of current injection or eddy currents, it is simply possible to increase the drive current into the sample until the signal rises from the noise, within the limitations imposed by SQUID dynamic range; all of the Vanderbilt data presented later in this paper utilized total drive currents of less than 100 milliamps! The Magneto-Optic eddy current Imager (MOI)[21] demonstrates that magnetic imaging is feasible on the flight line; SQUID magnetometry may offer the potential to achieve flaw detection with even greater reliability and sensitivity.

All of these factors, i.e. high temperature superconductivity, cryogenic refrigeration, the relative modest sensitivity requirements of SQUID NDE, and the demonstrated capabilities of noise cancellation techniques combine to make flight-line SQUID NDE feasible. However, preliminary aircraft NDE studies to date only show that the technique has promise; definitive demonstration of the sensitivity and reliability of SQUID for aircraft has yet to be accomplished. As we will describe below, the work at Vanderbilt has been directed towards the continued development of low temperature instrumentation and techniques to provide a rigorous evaluation of the potential strengths and weaknesses of SQUID NDE. The subsequent development of specialized SQUID NDE instruments suitable for use outside the laboratory, possibly utilizing high-T_c instruments, should allow the transfer of this new technology to the flight-line.

2. THE VANDERBILT SQUID NDE EFFORT

The Vanderbilt group has examined both experimentally and theoretically a variety of problems in SQUID NDE. We have developed a specialized Magnetic Imaging facility for studying the magnetic fields from biological and non-biological systems. We have imaged the magnetic fields produced by a wide variety of sources. In this review, we will discuss our various NDE measurements in the context of aircraft. The parallel effort in biophysics, particularly the imaging of cardiac action currents, is discussed elsewhere[22,23]. We have also developed analytical and numerical models that describe our measured magnetic fields, and we have developed inverse algorithms to allow us to deconvolve the fields to obtain images of the sources, whether they be distributions of current density or magnetization. We now describe each of these aspects of our work.

2.1 Instrumentation

The key hardware systems in the Vanderbilt Magnetic Imaging Facility are the MicroSQUID magnetometer[20], a magnetic shield[24], a scanning stage[25], and a computer control and data acquisition system[25]. The MicroSQUID magnetometer in Fig. 1 overcomes the limitations of previous biomedical SQUID systems by utilizing small (3 mm) diameter coils located close (within 1.5 mm) to room temperature samples. While the 90-100 fT/Hz$^{1/2}$ noise in Micro-SQUID is larger than in conventional SQUID magnetometers, the increased resolution and the reduced coil-to-source

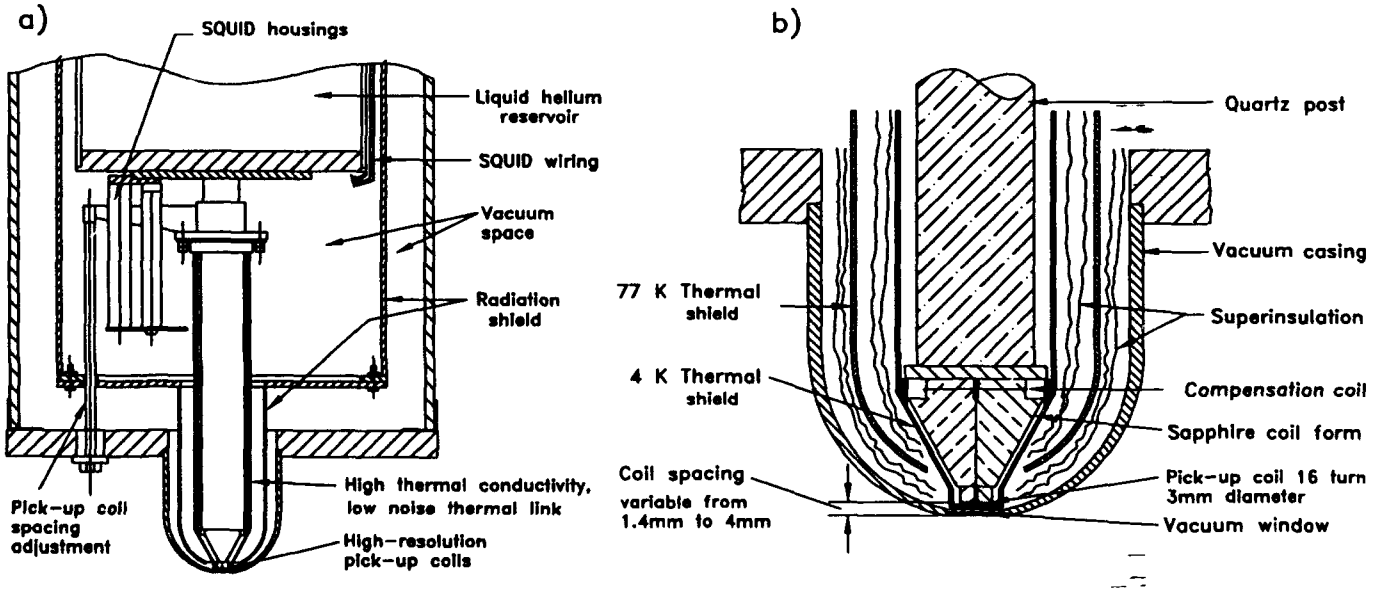

Figure 1. The Vanderbilt MicroSQUID magnetometer. Two views of the tail of the Dewar, showing the close spacing of the pickup coils to the outside of the dewar[20].

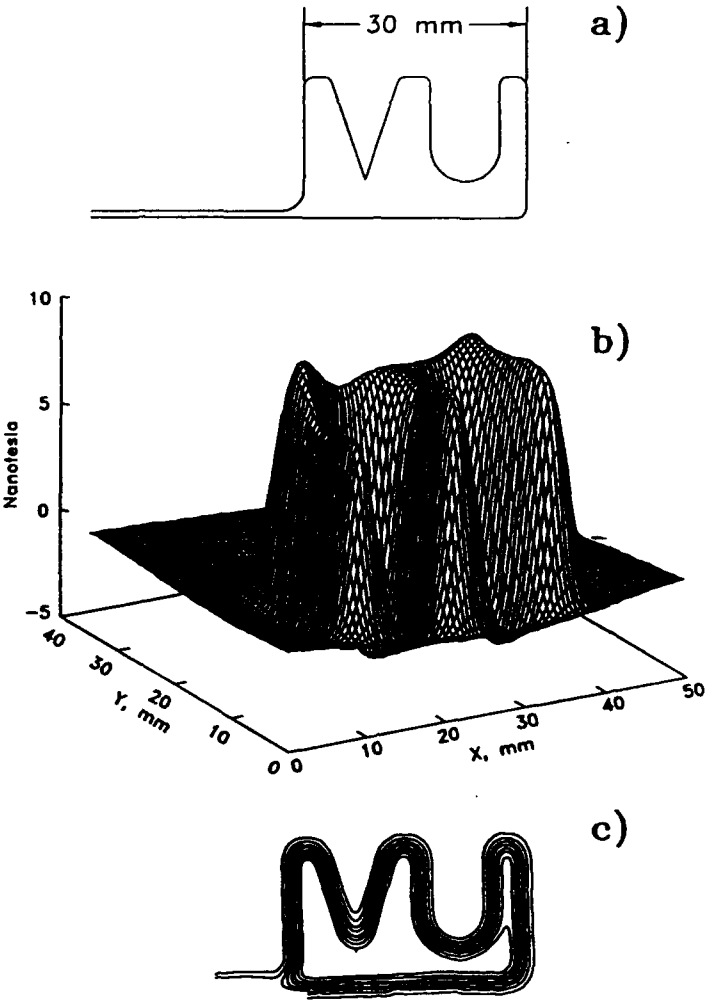

Figure 2. A test of the FFT imaging algorithm. a) A printed circuit pattern carrying a 100 μA DC current. b) The magnetic field map measured by MicroSQUID with the 3 mm diameter pickup coils positioned 2.5 mm above the circuit. c) The current image obtained from the data in b) using unconstrained FFT deconvolution (12.5 μA per line). Adapted from Ref. 25.

spacing more than compensate to provide low-noise, high-resolution images[26]. Multiple SQUID channels allow real-time spatial filtering that is optimized for the particular source being studied, while at the same time improving the signal-to-noise ratio. The magnetic shield provides sufficiently low noise (8 fT at 10 Hz) and high 60 Hz attenuation (10^6) that it serves as an essentially noise-free SQUID NDE test facility. The first computerized, nonmagnetic translation stage for scanning samples beneath MicroSQUID, with its 50 × 50 mm range and 1 mm/s velocity, has just been replaced by a high speed (20 cm/s), 22 cm × 66 cm stage.

2.2 Image processing

The success and acceptance of many NDE techniques such as radiography, ultrasound C-scans, ultrasonic microscopy, and X-ray tomography have been aided by the presentation of two-or even three-dimensional images of the test object and the flaws that it contains. However, the lack of an image has not prevented the widespread acceptance of conventional eddy-current and ultrasound instruments, for which the nature of the measurement often provides a characteristic, qualitative signal or signature rather than a quantitative image of the flaw. With SQUID NDE, the uniformity of the applied magnetic field or current, the accuracy with which the SQUID can map the field above the test object, and the ease with which any distortion of these fields by the unflawed portions of the object can be eliminated make quantitative flaw imaging an attractive capability of the technique.

We have previously demonstrated that two-dimensional magnetic images can be deconvolved into images of current or magnetization by filtering techniques carried out in the spatial frequency domain[27], as was done for the test pattern in Fig. 2. However, with this approach, it is difficult to utilize *a priori* information such as the known geometry of the irregular borders of the sample. The need to constrain images can be readily met through a finite element imaging technique[28,29], illustrated in Fig. 3. Other imaging approaches include lead field analyses[28], maximum entropy methods, iterative approaches[30], and others that are under investigation at Vanderbilt and elsewhere.

Different deconvolution algorithms have their own merits in dealing with certain kinds of sources. As we will show in the following sections, we have applied appropriate algorithms to magnetic field data produced by a planar current-carrying conductor with flaws, and by the diamagnetic magnetization of plexiglass. As an example of the differences between techniques, the finite element method can constrain the solution to a finite extent, but is

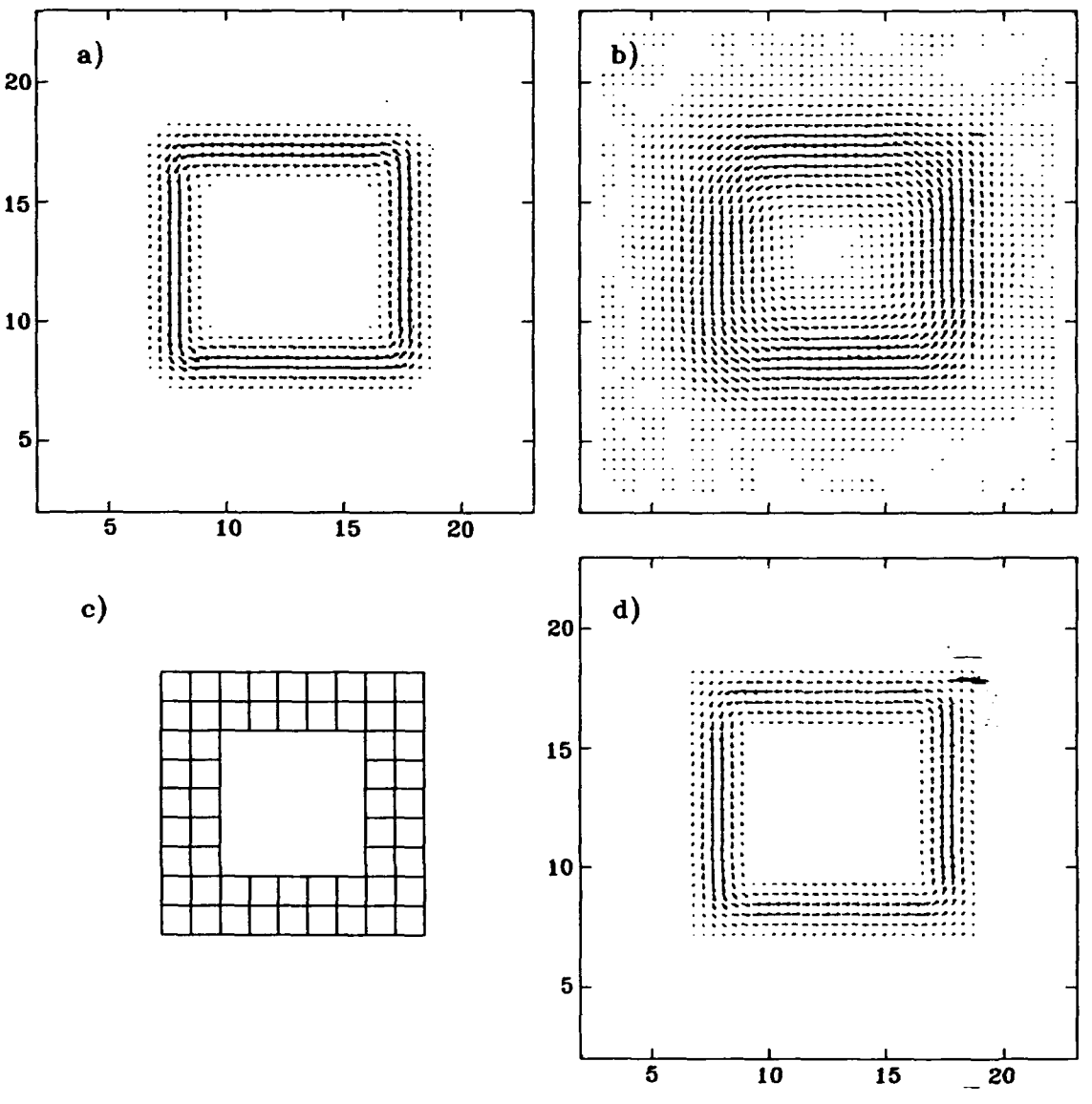

Figure 3. FFT and finite element deconvolution. a) A numerical test current pattern. b) An unconstrained FFT reconstruction of the currents from simulated magnetic fields 3 mm above the pattern with 20% noise (Mean square deviation = 0.42). c) A constrained finite element mesh defining the conductor borders. d) A finite element reconstruction from the same magnetic data (MSD = 0.122). Adapted from Ref. 29.

sensitive to the imperfections in the input data. The maximum entropy method is more stable for fitting noisy data but may not find the best solution for data with a high signal-to-noise ratio. For cylindrical geometries, a lead field analysis provides a simpler algorithm. Each of these algorithms has advantages for particular problems while being inadequate for others. However, with all the approaches, the deconvolved source images are easier to interpret than the original magnetic field data[29]. Whether a complete image or simply a characteristic signal are required to detect a flaw may depend upon the specific application being addressed; in either case, our preliminary studies indicate that one of the advantages of SQUID NDE is that it provides quantitative data that can be viewed directly or analyzed by measurement models.

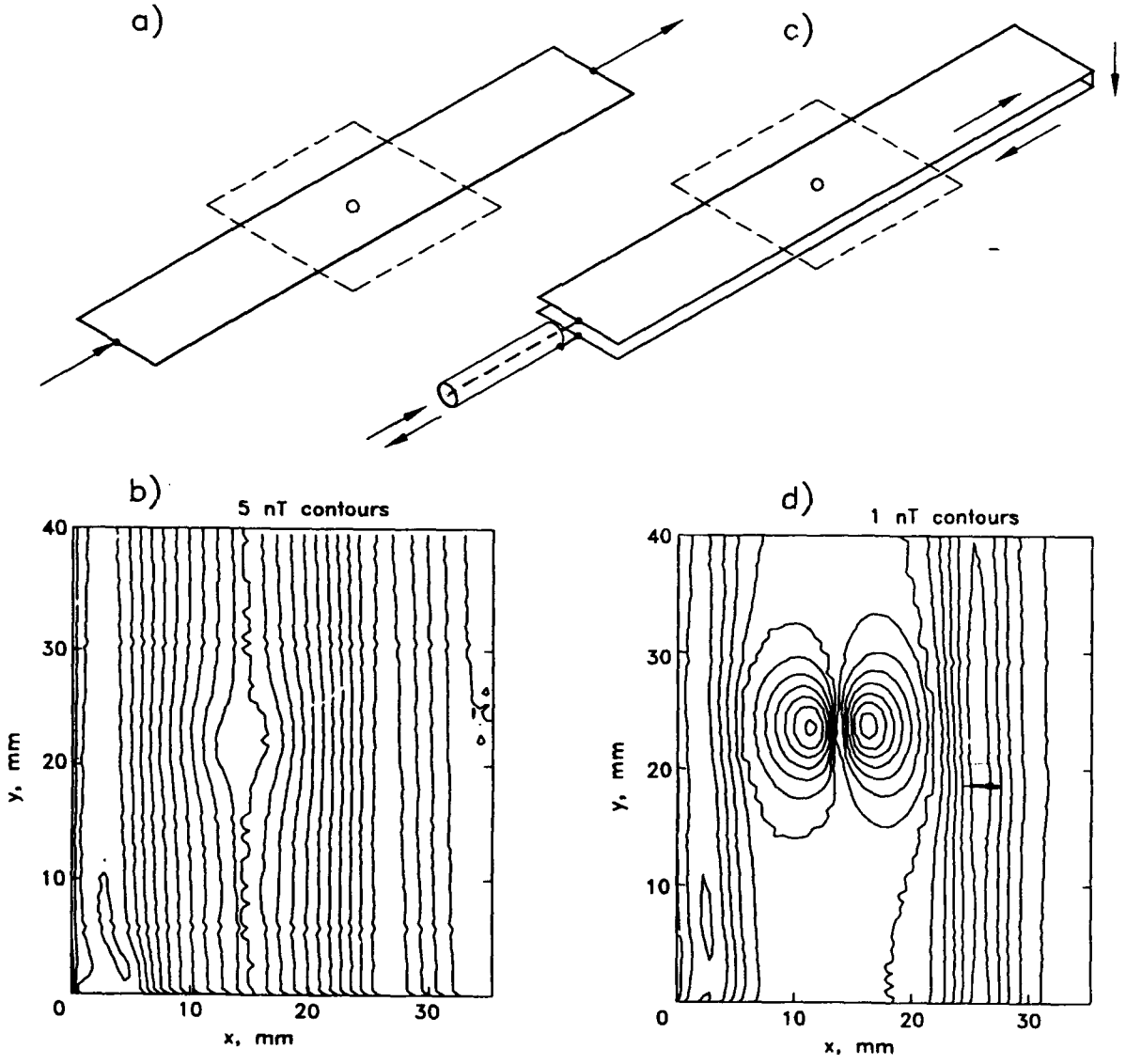

Figure 4. Cancellation of background signals. a) A 25 mm × 150 mm × 32 μm copper sheet with a 3 mm diameter hole at its center. A 7.5 mA, 1.6 Hz current was applied through contacts at each end. The dotted square represents the region scanned by MicroSQUID. b) An isofield plot of the normal component of the magnetic field over the region indicated by the dotted square in (a). The major variation was due to the field from the plate edges, while the small variation at the center was due to the hole. c) The canceling technique as applied to the conductor in (a). The unflawed canceling plate was 450 μm beneath the conductor in (a), and carried an equal and opposite current. The two conductors were connected to the power supply by a coaxial cable. d) An isofield plot for the magnetic field in the dotted square in (c). Note the increased scale as compared to (b). Adapted from Ref. 32.

2.3 Experimental studies

2.3.1 Injected current imaging. Weinstock[1] first demonstrated the ability of a SQUID magnetometer to detect flaws in conducting objects by observing the magnetic fields associated with the perturbation in an applied electric current as it is deflected by the flaw. Unfortunately, when this technique is applied to flaws in planar conductors, the signal from the flaw can be masked by that of the currents in the conductor and the lead-in wires, even though the flaw signature is well above the noise[31]. This limitation has been overcome by a technique developed at Vanderbilt in which an unflawed conductor carrying an equal and opposite current distribution is placed adjacent to the test surface[32]. As shown in Fig. 4, this allows the current to be delivered by a magnetically-silent coaxial cable, and eliminates most of the background magnetic field due to the currents in the unflawed sections of the test plate.

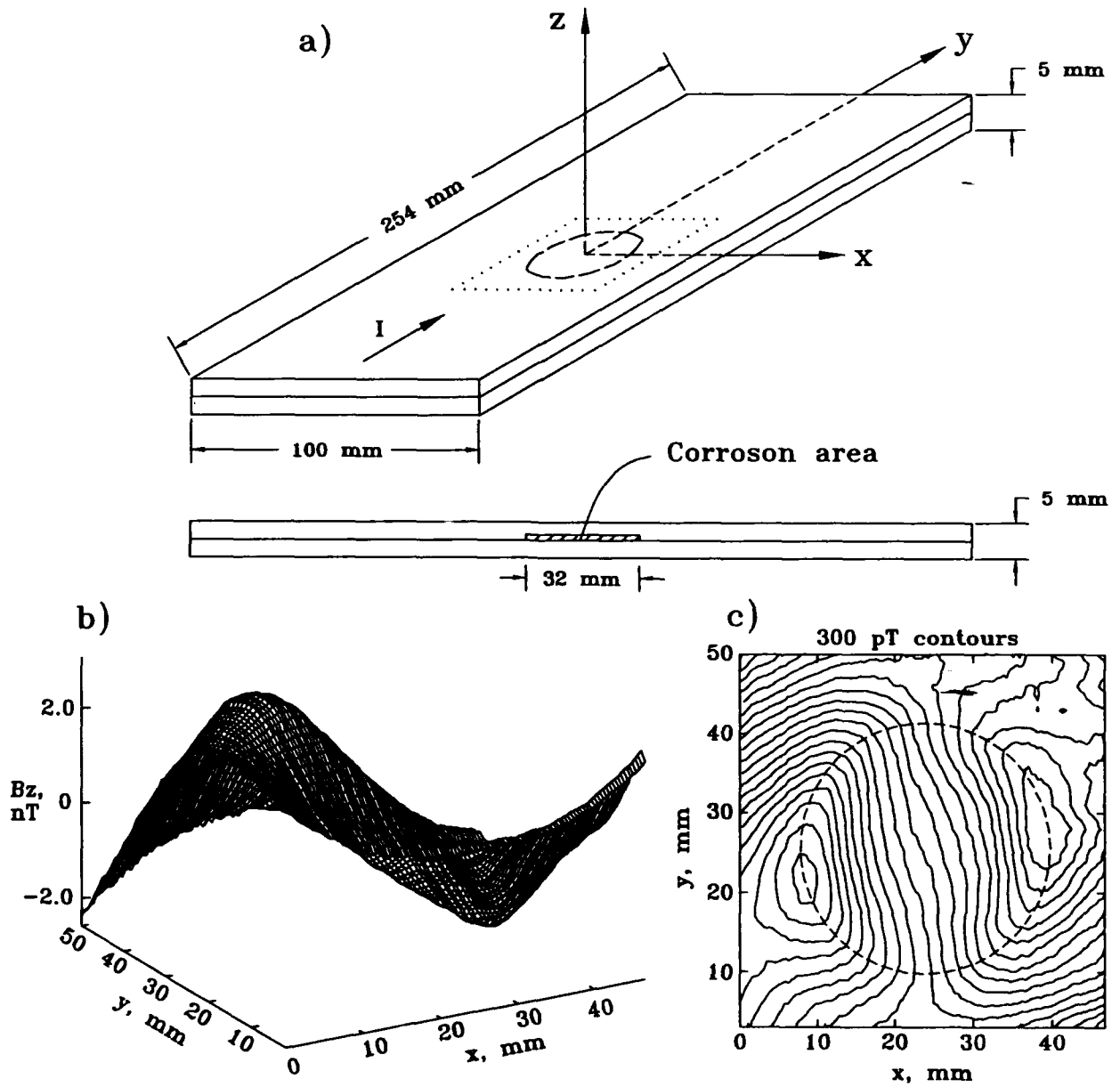

Figure 5. SQUID imaging of hidden corrosion. a) A simulated lap joint in an aircraft wing surface, consisting of two insulated aluminum plates. Standard eddy current analysis indicates a 2% mass loss in the corroded area. A 10 Hz 58 mA AC current was injected into the plate. b) and c) Magnetic images; the dashed line shows the hidden flaw. From Ref. 34.

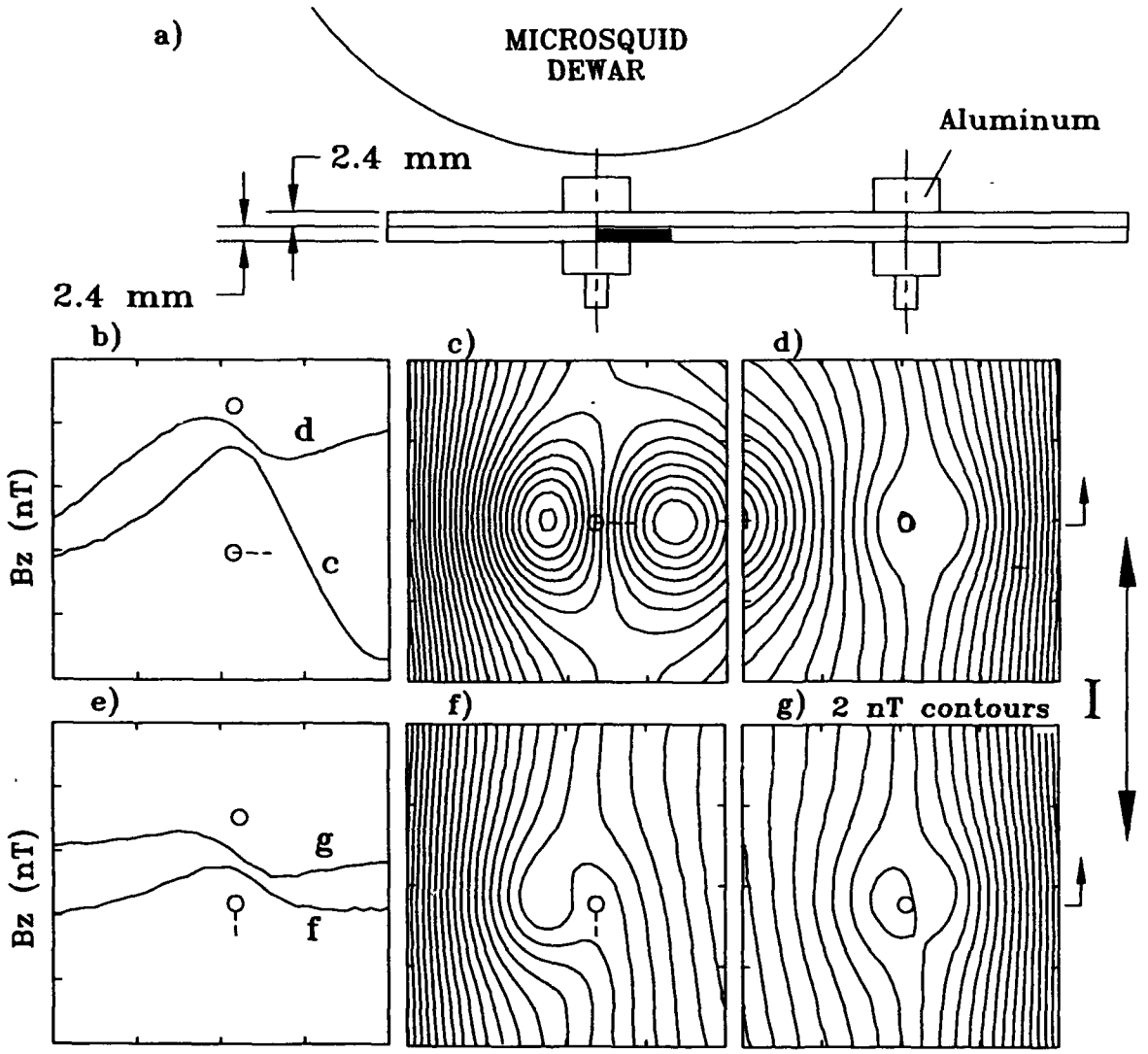

Figure 6. SQUID detection of second-layer cracks. a) A test sample of two 7075-T6 aluminum panels bolted together by six aluminum pins and nuts. Each panel is 250 × 100 × 2.4 mm thick. For three pins, second-layer cracks are simulated by EDM slots in the bottom layer adjacent to the rivets. The slot width was less than 0.4 mm. The SQUID pick-up coil is located 3 mm above the rivets (4.5 mm above the plate). 47 Hz 30 mA current was injected into the plate and the magnetic field 3 mm above each pin was measured with MicroSQUID. c), d), f), and g) Isofield contour plots for four different rivets. b) and e) Corresponding field profiles through the rivets. The crack in (c) is 12 mm (1/2 in) long and transverse to the current; while in (f) it is parallel to the current. Scans (d) and (g) are for adjacent, unflawed holes with rivets. The differences between the flawed and unflawed holes with rivets are evident in the current profiles (b) and (e) along a horizontal line through the holes. Adapted from Ref. 34.

In collaboration with Lockheed[33], we have begun to apply our techniques to the aging aircraft problem. Figure 5 shows magnetic data recorded from Lockheed-prepared aluminum samples that simulate lap joints in aircraft wings[34]. Injection of a 58 mA, 10 Hz current allowed detection of a hidden, 16 mm radius corrosion area, whose mass loss was approximately 2% according to eddy current analysis. As shown in Fig. 6, our technique is also capable of discriminating between the current perturbation caused by an aluminum fastener and that caused by a 6.4 mm long EDM slot immediately adjacent to the fastener. By varying the frequency of the injected current, it is possible

to adjust the maximum depth sensitivity of the technique: at 10 Hz, the skin depth, δ, is 4 cm in 7075 Al, and so sensitivity is limited only by the $1/r^2$ dependence of the field due to the flaw. As we will discuss later, the width of the signature is directly related to the depth of the flaw, and the strength of the signature to its size and orientation. The deconvolution algorithms discussed above can also be used to obtain images of the current distribution in the sheet for both flawed and unflawed second-layer rivets, presented in Fig. 7, which show how the current pattern is both displaced to the left and covers a larger region because of the EDM slot on the left side of the rivet.

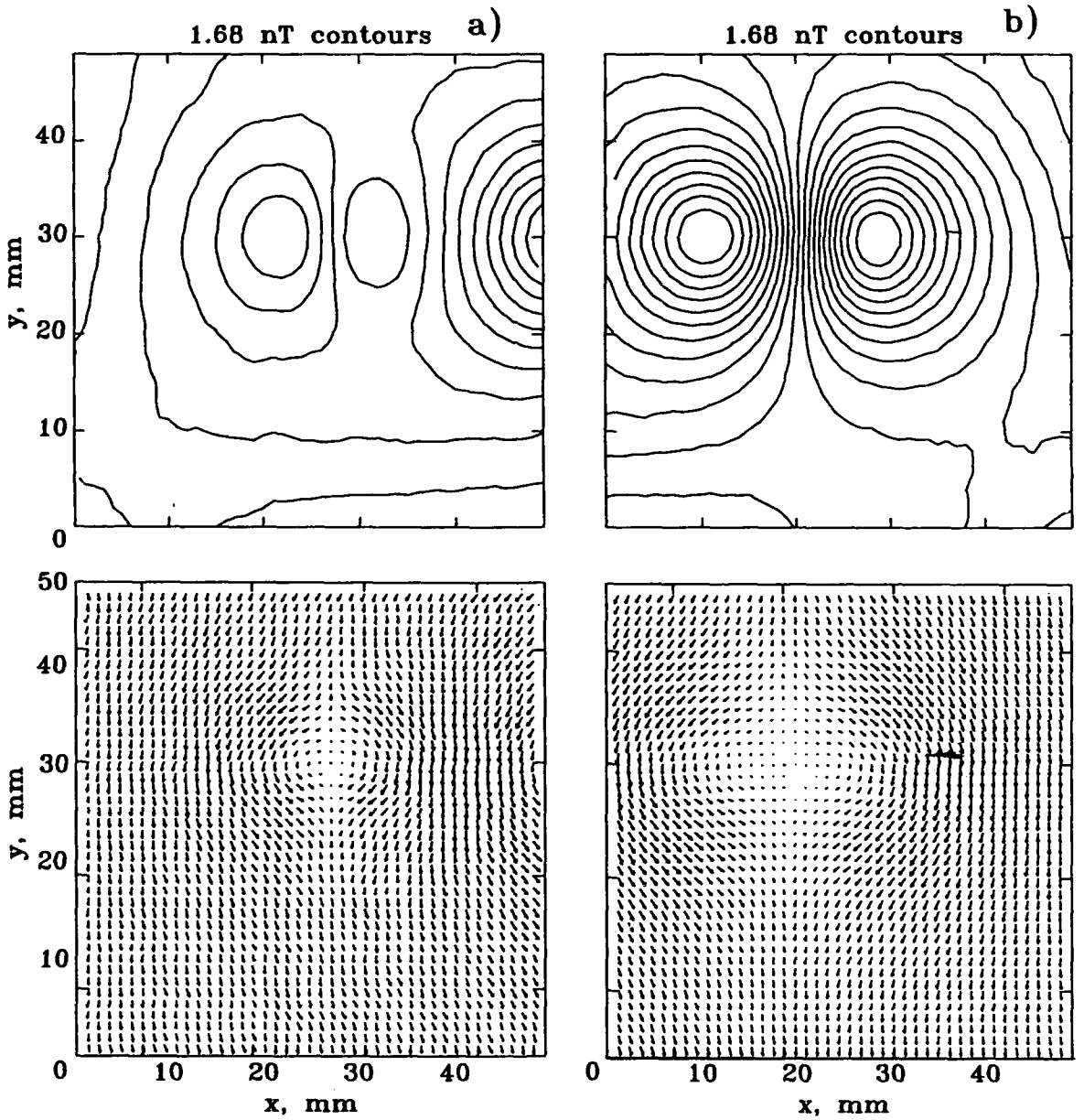

Figure 7. Field maps and current images of rivets. Measured magnetic field contour map (above) and computed current density arrow map (below) due to current injection into a pair of conducting plates containing rivets without flaws (left) and with second-layer flaws (right). From Ref. 28.

We have examined a 1.1 mm thick test plate[35] with a 1 mm long crack located entirely within the countersunk region for a flush-mounted rivet[36]. An injected current density of only 2.5 mA/cm^2 was required to produce the images in Fig. 8. By imaging the magnetic field for current parallel to the crack, we can estimate the signature from an unflawed rivet hole. There is a clear difference between the magnetic images 8d and 8e, with the peak to peak amplitude and the separation of the peaks in 8f being significantly larger for the case where the current has to flow around the crack. The pair of loops in the FFT current image in Fig. 8g may be the actual image of the two cracks, but the more detailed analysis of the imaging process will be required before we are able to interpret this image fully. Analysis of images recorded at a frequency of several hundred Hz suggests that it may be possible to achieve selective depth sensitivity that enhances the crack signature[57], but, again, more theoretical analysis is required.

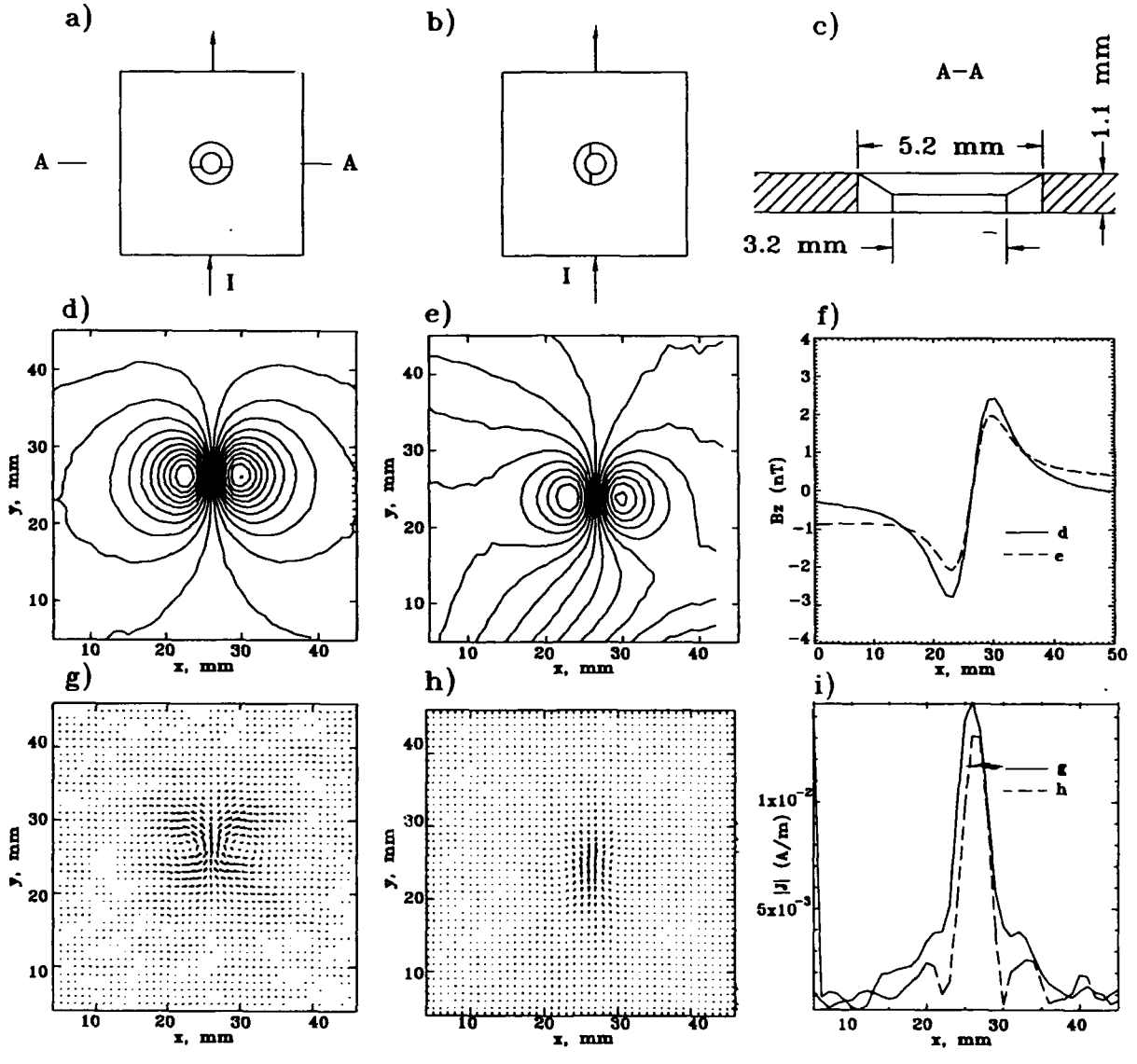

Figure 8. SQUID detection of cracks within a rivet countersink. Test specimen with EDM machined slots that do not extend beyond the countersink of the rivet hole[35]. a) and b) Two orientations of applied current. c) Sample cross-section. d) and e) Isofield maps for currents injected perpendicular and parallel to the slot. f) Field profiles showing the detectability of the slots. g) and h) Current images computed from (d) and (e) using the FFT algorithm. i) Current profiles through the flaw.

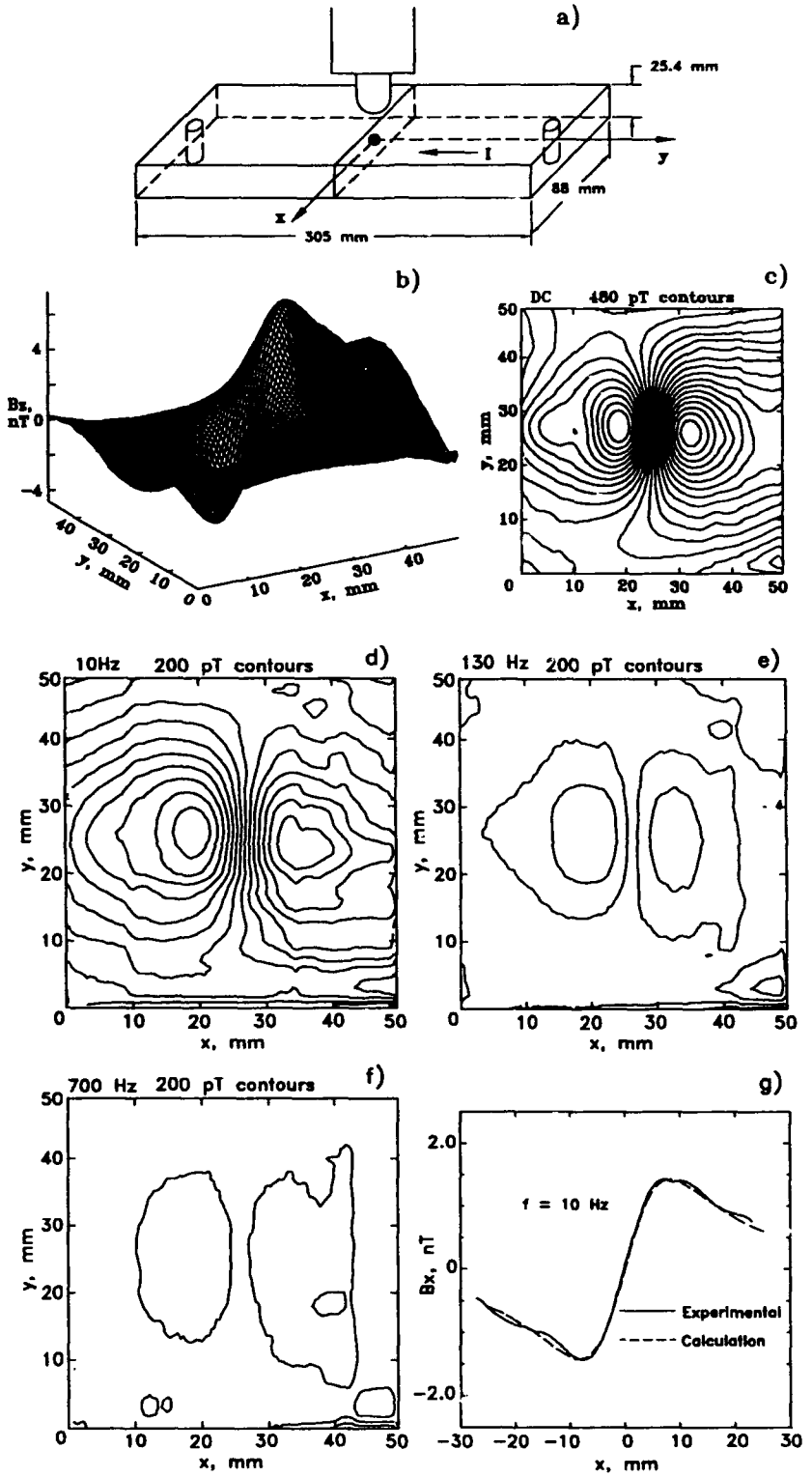

Figure 9. SQUID imaging of deep flaws in metals. a) A 4.7 mm radius spherical cavity inside a 305 × 88 × 25.4 mm rectangular brass bar carrying 70 mA of DC current along its length. The cavity is located 7.9 mm below the top surface. b) Surface and c) isofield contour maps of the magnetic field. d,e,f) Maps for 10, 130, and 200 Hz AC currents, respectively. g) Theoretical and experimental field profiles. Adapted from Ref. 37.

Subsurface flaws in electrically conducting components are difficult to detect by conventional eddy current techniques because of the skin depth, δ, at high frequencies. However, SQUID magnetometers are capable of imaging DC and low-frequency magnetic fields, thereby allowing sources to be detected deep inside conducting samples. A spherical flaw beneath the surface of a brass bar has been detected by injecting both DC and low-frequency AC current. Figure 9 shows magnetic images for a spherical cavity with a 4.7 mm radius inside a 305 mm long × 88 mm wide × 25.4 mm thick rectangular brass bar[37]. At DC, the flaw is readily imaged. By injecting AC current with several frequencies, we can estimate the depth of the flaw. At frequencies above 200 Hz, the flaw is practically invisible, indicating the potential benefits of SQUID-based extra low frequency eddy current (ELF-EC) techniques.

2.3.2 Eddy current imaging. While the injected-current technique is useful for high-precision measurements on test samples, the need to make good electrical contact with the sample would make it difficult to use the technique on actual aircraft structures, particularly if they are painted. We have adapted a standard eddy-current technique, also used in the Magneto-Optic Imager[38,39], in which the AC magnetic field is applied by a sheet conductor parallel to the test surface. This induces a large-extent sheet current in the test specimen, and thus produces flaw perturbation fields quite similar to those obtained with direct current injection[34]. SQUID data from this technique are shown in Figs. 10, 11 and 12, confirming that this approach is valid for hidden corrosion, closed fatigue cracks, and second-layer cracks at rivets.

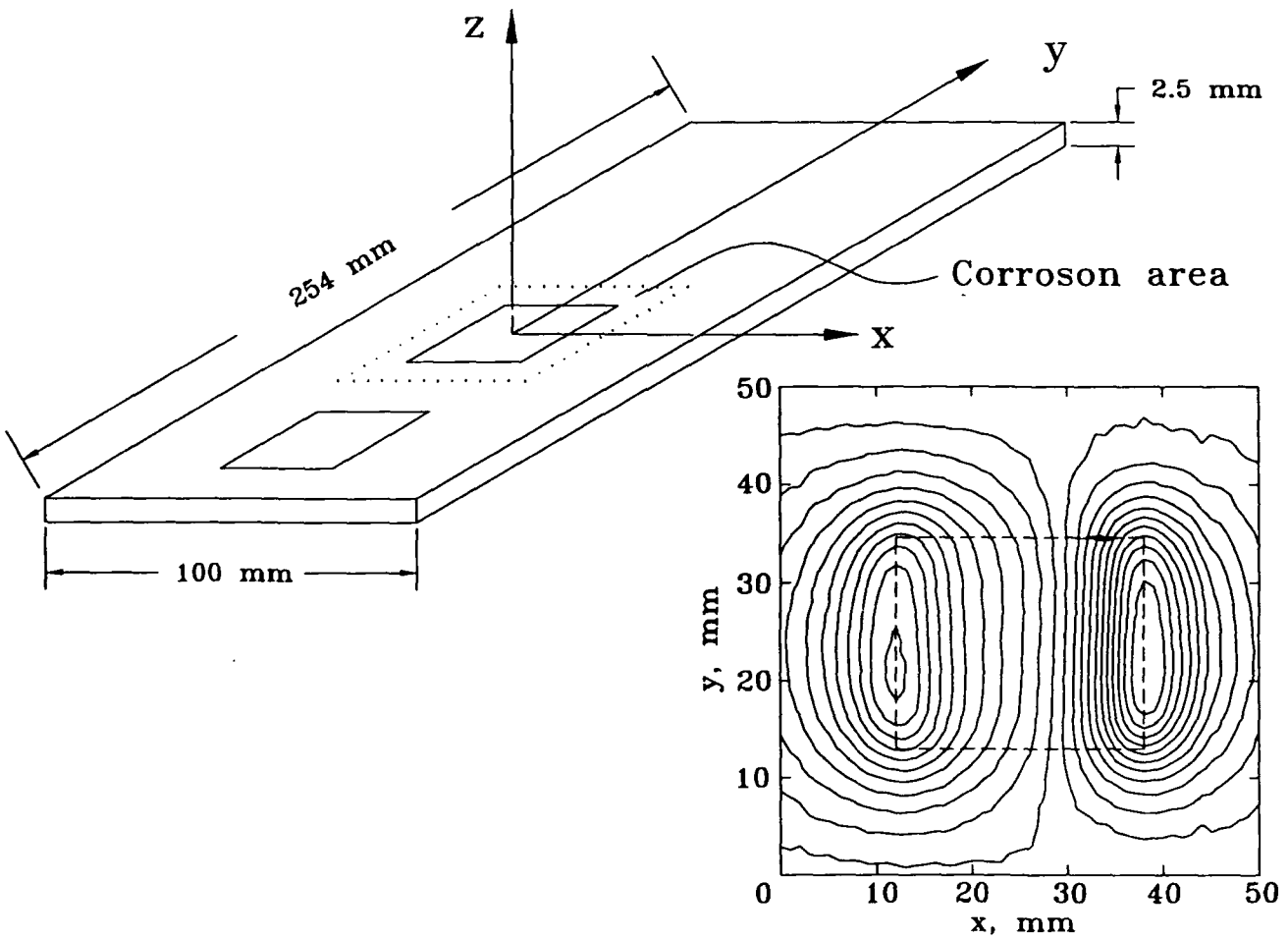

Figure 10. SQUID eddy current image of corrosion. a) An insulated, 2.5 mm thick aluminum plate. The 26 mm × 21 mm corrosion area is open on the surface, and is less than 1 mm deep. Another flat, current-carrying plate between the SQUID and the test sample is used to induce the eddy currents, whose magnetic field is shown in b). The flaw could be imaged from either side.

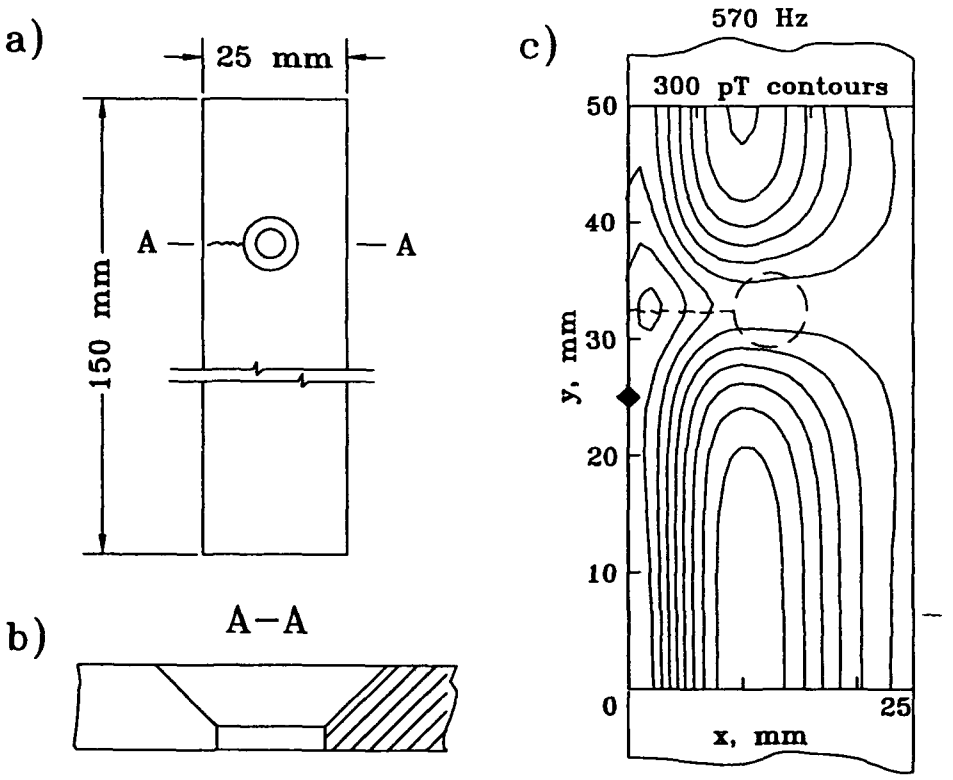

Figure 11. SQUID imaging of a closed fatigue crack. A MicroSQUID image of the magnetic field produced by the perturbation in induced currents that results from a closed fatigue crack half-way across a 25 mm × 2.3 mm aluminum strip with a rivet hole[35]. a) Plan and b) cross-section views. c) Isofield contour map.

2.3.3 Magnetic susceptibility imaging. The SQUID NDE techniques that we have described so far are limited to conducting objects. While these techniques should be well-suited for the detection and quantification of second-layer cracks and corrosion in aging aluminum-skin aircraft, they will be of little use for aircraft fabricated using advanced non-metallic composites or ceramic materials. Ultrasound C-scans are useful for finding internal voids in planar sheets of fiber/resin composites, but the utility of ultrasound as a NDE tool is compromised for complex structured shapes, largely because of the difficulty in maintaining the transducer in good acoustical contact with the material, because of internal reflections and scattering of the acoustic waves by curved surfaces and internal boundaries, and because of lack of contrast between some impurities and the base material. X-ray techniques are limited by the low x-ray attenuation coefficient of many of these materials, resulting in minimal contrast between a void and the adjacent solid material. Other studies demonstrated that SQUID mapping of remanent magnetic fields can be used to study objects with intrinsic ferromagnetic impurities or extrinsic ferromagnetic decoration[31,40,41], but the inverse imaging problem for these measurements is insolvable because of the lack of knowledge regarding the direction of magnetization of the ferromagnetic material.

Several of these difficulties may be overcome using magnetic susceptibility imaging and tomography techniques developed at Vanderbilt[42,43,44,45,28]. We have shown experimentally and theoretically how SQUID magnetometers can be used in conjunction with an applied magnetic field to image spatial variations in the magnetic susceptibility of diamagnetic and paramagnetic objects. In order to demonstrate the feasibility of this technique, we have attached a pair of Helmholtz coils to our high resolution MicroSQUID magnetometer so that we can apply a nearly uniform field of 0.3 mT, 2 mm below the 3 mm diameter sensing coils[43]. By placing a small sample in this applied field and scanning, MicroSQUID measures the local magnetic field variations caused by the spatial distribution of magnetic susceptibility in the sample. The system has sufficient sensitivity to image susceptibility-induced field changes equal to 3×10^{-10} of the applied field, in a 1 Hz bandwidth.

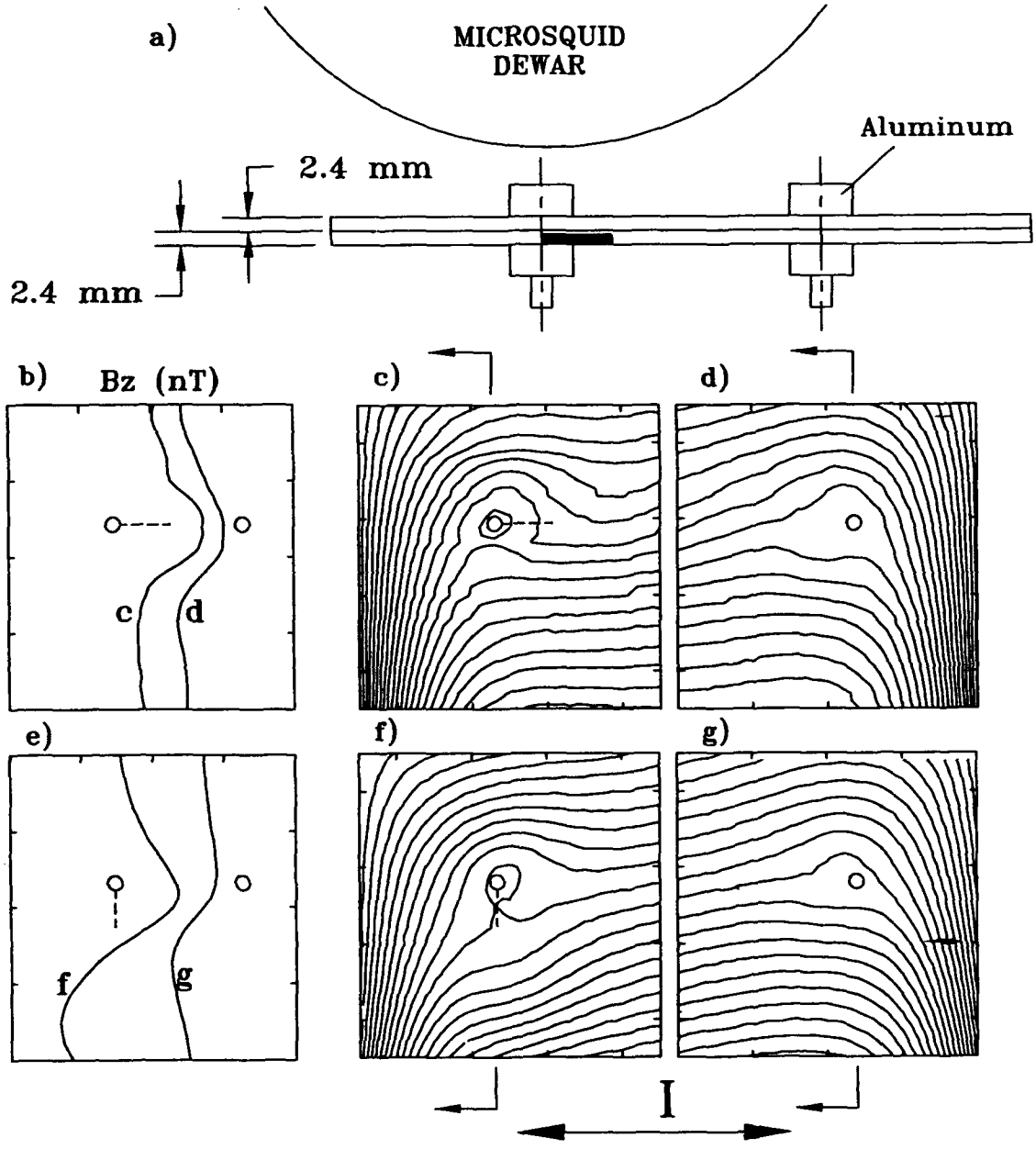

Figure 12. SQUID eddy-current detection of second layer cracks. For the same sample as in Fig. 6, a flat, current-carrying plate between the SQUID and the test sample was used to induce 340 Hz eddy currents across the sample strip. c), d), f), and g) Isofield contours for four different rivets. b) and e) Corresponding field profiles through the rivets. The crack in (f) is transverse to the current while that in (c) is parallel to it. The holes in (d) and (g) are unflawed. The differences between the flawed and unflawed holes are evident in the current profiles (b) and (e) along a vertical line through the holes. Adapted from Ref. 34.

To test the capabilities of this technique for imaging two-dimensional distributions of magnetic susceptibility in thin samples, we imaged complex shapes of plexiglass, scanned in a uniform applied field. Deconvolution of these data[28] yielded susceptibility distributions that were accurate images of the samples, as shown in Fig. 13. We found that the susceptibility of this plexiglass sample was -9.0×10^{-6} (SI) and demonstrated[44] that our system is sensitive to susceptibility contrasts as small as 5×10^{-7} (SI), with a spatial resolution on the order of 1 mm. We have also shown that this technique can be used to obtain high quality images of the heterogeneous magnetic susceptibility and remanent magnetization of a 50 μm thick slice of volcanic rock[46]. The performance of the MicroSQUID implementation of this concept is limited by the strength of the applied field, by the size and distance of the sensing coils from the sample, and by SQUID noise. We estimate that we could increase spatial resolution by a factor of two, and sensitivity to susceptibility contrast by at least one order of magnitude by using an imaging susceptometer whose SQUIDs are integrally mounted within a superconducting magnet. Such a system in presently under construction for our studies.

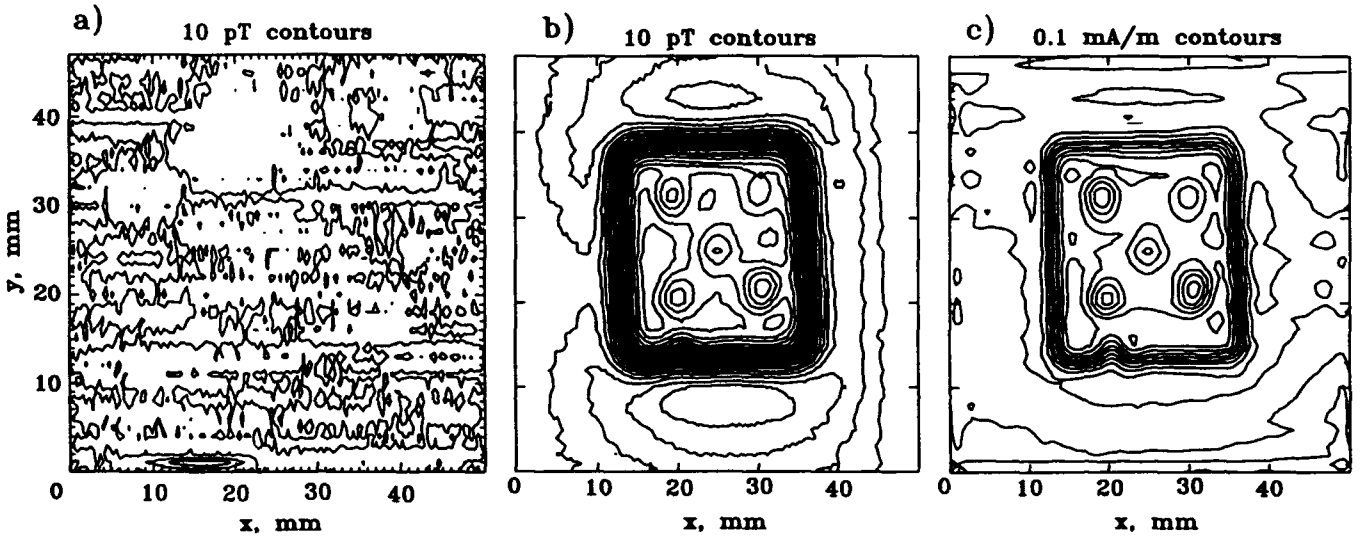

Figure 13. A magnetic image of plexiglas. The sample is a 25.4 × 25.4 × 6.3 mm high block of plexiglas (susceptibility = -9.0×10^{-6}, SI) with five 1.8 mm diameter holes drilled through it. a) The magnetic field recorded above the specimen with no applied field. b) The magnetic field measured with an applied field of 114 μT. c) The 2-D magnetization image calculated by FFT deconvolution of the magnetic field perturbations measured 2.5 mm above the block in the presence of an applied field. The five peaks do not extend to the zero magnetization level because of the FFT algorithm and the limiting resolution of the 3 mm sensing coils of the SQUID. From Ref. 44.

We have also shown theoretically that the application of the magnetic field from multiple directions and the recording of the diamagnetic perturbation signals over the entire surface of the object can be utilized to obtain a three-dimensional tomographic reconstruction of the internal susceptibility distribution of the object[42], overcoming the famous non-uniqueness of the magnetic inverse problem. To obtain the three-dimensional susceptibility distribution X, we solve the system of equations B = G * X, in which B is the set of magnetic field measurements and G is the matrix of Green's functions that must be inverted. In many cases, the solution is non-unique, but we overcome this problem by measuring the magnetic field in several different planes close to the sample while applying the magnetic field sequentially from multiple directions. The resulting system of equations is overdetermined and singular value decomposition techniques, among others, can be used to reconstruct the 3-D susceptibility distribution. Our preliminary studies show that with two of the three strategies investigated, the algorithm can correctly discriminate between

voxels with susceptibilities differing by only 5×10^{-6} (SI). Since this preliminary numerical simulation utilized only a small number of sample orientations and a single magnet/SQUID configuration, in contrast to the hundred or more projections for X-ray tomography, we anticipate a significant improvement in both the sensitivity and spatial resolution of magnetic susceptibility tomography when more advanced algorithms and measurement protocols are developed.

Detection of surface flaws in critical metallic components is currently performed by eddy current techniques, or by visual analysis of fluoro-penetrants. Acoustic microscopy is used as a research tool. However, these methods are often limited by low sensitivity, poor spatial resolution, or slow throughput. Some are ill-suited for ceramics. All of these limitations are addressed with an alternative technique involving decoration of the non-ferromagnetic samples with a ferromagnetic or superparamagnetic penetrant and subsequent scanning with a high-resolution magnetometer or susceptometer. Figure 14 presents our preliminary data that demonstrated that this technique is sensitive enough to detect, with a 10 to 1 signal-to-noise ratio, defects at least as small as 250 μm long $\times$ 50 μm wide $\times$ 75 μm deep in a nickel test block[45]. Applied field strength and SQUID noise will ultimately limit sensitivity, and sensing coil characteristics will limit spatial resolution. We expect that the imaging susceptometer presently under construction will improve the sensitivity to the point where a large-coil SQUID may provide both rapid and sensitive scanning of ceramic bearings in which microscopic surface flaws have been decorated with superparamagnetic tracers.

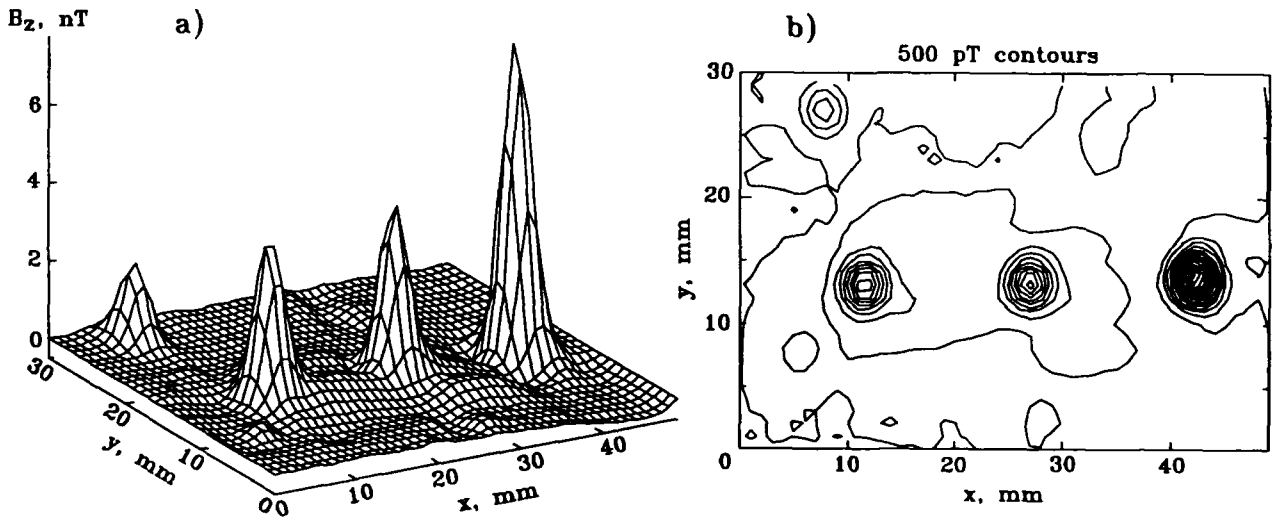

Figure 14. Surface decoration with superparamagnetic microspheres. Two plots of the magnetic field measured 2.5 mm above a block of nickel alloy containing three EDM surface defects that are 500 μm long and 50 μm wide with various depths (left: 150 μm; middle: 230 μm; right 300 μm), that is exposed to a 171 μT applied field. A solution of superparamagnetic microspheres was applied uniformly to the block and its surface was then wiped clean. The field from the susceptibility of the block was removed by subtracting the field measured before application of the spheres from that measured afterwards. From the strength of the signal, the small defect in the upper left corner was found to have a volume of $1.9 \pm 0.6 \times 10^{-12}$ m^3 and was subsequently identified through microscopic examination to be a relatively deep scratch approximately as long as the left-most EDM slot. Adapted from Ref. 45.

Magnetic susceptibility imaging offers promise as a new method for imaging composites, either through surface or three-dimensional tomographic imaging to determine regional variations in susceptibility arising from voids, unpolymerized resin, or differences in the relative concentrations of chemical components, or through the use of ferromagnetic or superparamagnetic penetrants. Since the approach is relatively new and untested in realistic aircraft specimens, it is premature to speculate whether this approach will be of use for NDE of non-metallic composite aerostructures.

2.4 Theoretical studies

We have developed analytical and numerical models for the simulation of flaws with several geometries inside thick and thin, current-carrying plates and thin-walled tubes. These models have been used for locating and sizing flaws in test samples, and will serve as the basis of future measurement models. Although the geometry of real flaws is not in general simple, the analytical solutions for the three ideal geometries we have considered can be used for estimating the size, orientation and location of a flaw faster than can numerical calculations, and also, they can be used to determine the accuracy of more realistic numerical calculations that describe complicated geometries.

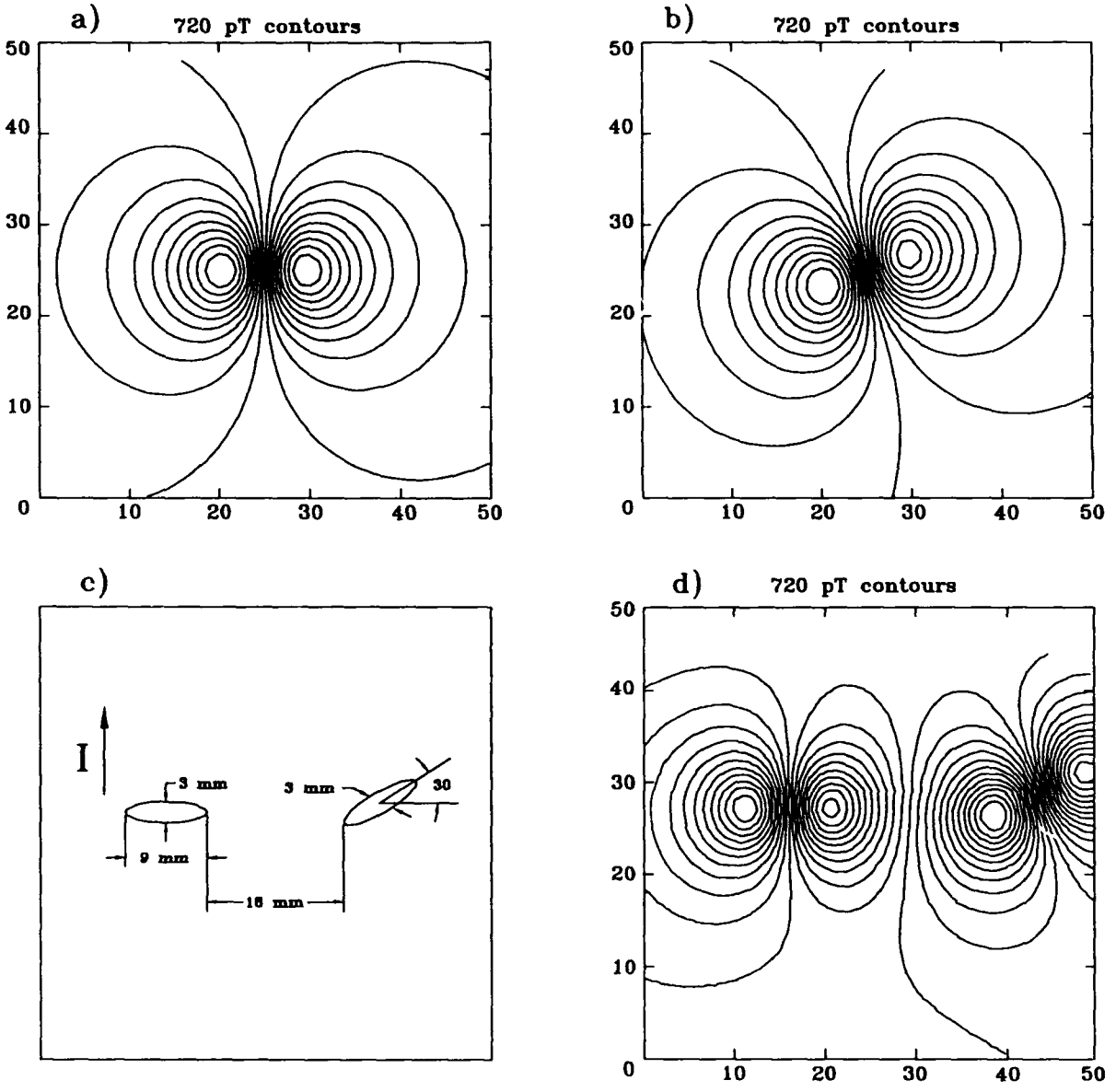

Figure 15. SQUID imaging of flaws in metals. a) B_z calculated for a 9 mm × 3 mm ellipse in a 2 mm thick aluminum plate carrying a current density of 2.5 mA/cm^2. The major axis of the ellipse is horizontal. b) The same as (a), except that the ellipse is rotated 30°. c) Ellipse geometry. d) MicroSQUID-measured isofield map for the ellipses in (c). Adapted from Ref. 34.

2.4.1 Elliptical holes. We have calculated two dimensional current distributions due to elliptical holes in a conducting plate, and have then used this distribution to calculate the magnetic field from flaws in both thin and thick conducting plates. An analytical solution has been found to describe the magnetic field for a thick plate[47], which, to our knowledge, has not been previously reported. This model can be used to determine the size, location and orientation of a crack in a current carrying conductor by setting to zero the length of the minor axis of the ellipse.

As an example of this model, Figs. 15a and b show the calculated contour maps of the magnetic field in the z direction 3.0 mm above the plate for two orientations of the ellipse. The plate is 2.0 mm thick and is carrying current density 2.5 mA/cm^2. To confirm the calculations, we have mapped the field for two ellipses with major axes 9 mm and 12 mm, and minor axes 3.0 mm, which are oriented at 90° and 60° with respect to the current (see Fig. 15d). While the ellipses are not perfect and also are slightly different from those used in the model calculations, the test data are in good agreement with the model predictions. Most importantly, the model shows that for large flaws, the magnetic field contains information about the shape of the hole relative to the direction of the applied current: the fact that the right-most hole is tilted with respect to the applied current is evident in the tilt of the field pattern.

2.4.2 Circular holes. To examine the effects of hole size on the observed magnetic images, we have made an extensive series of analytical and finite-element calculations of the magnetic field produced when current is passed through a metal sheet containing circular flaws[48]. We have previously demonstrated the difference between imaging resolution and localizing resolution[49], and we showed that when the flaws were significantly smaller than the distance between the flaw and the SQUID, i.e. the SQUID was in the far field of the flaw, the magnetometer could localize

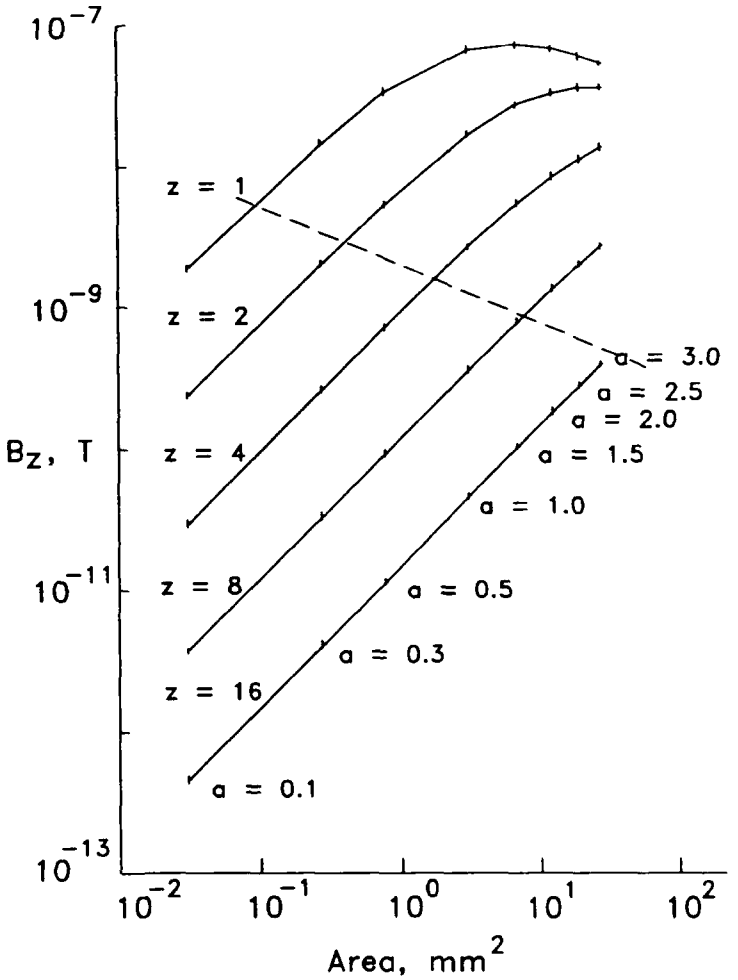

Figure 16. Proportionality of magnetic field to hole area. Variation of the normal component of the magnetic field B_z as a function of hole area in a conducting plate at various measurement heights, z (in mm). The hole radius ranges from 0.1 to 3 mm. In the far field limit where the holes are small as relative to the pickup coil distance (below the dashed line), B_z varies linearly with hole area. From Ref. 48.

the flaw but not image it. The most important finding illustrated in Fig. 16 is that in the far field (below the dashed line), the peak-to-peak amplitude of the flaw signal was directly proportional to the area of the flaw. In addition, the separation between the positive and negative extrema in the magnetic field image was $\sqrt{2}$ times the depth of the flaw beneath the magnetometer measurement plane. Thus if a flaw was smaller than the imaging resolution of the SQUID magnetometer, the flaw size could still be determined accurately. For flaws in the near field, the flaws could actually be imaged and their exact shape and size determined.

2.4.3 Other geometries. We have also developed mathematical models for simulation of flaws of different shapes inside a thick current-carrying plate. We have calculated the three-dimensional current distribution due to a finite-depth cylindrical flaw in a thick current-carrying plate[50]. *In general, it is difficult to solve this kind of boundary value problem analytically.* We have found an analytic solution by introducing a test function, from which the magnetic field is derived, although the calculations are rather involved. A three-dimensional current distribution due to a spherical flaw inside a thick current-carrying plate has been calculated by the method of images[51]. We have found an analytical solution, which has not been reported before, to calculate the magnetic field due to the spherical flaw. This solution has been successful for simulating the magnetic field produced by a spherical cavity inside a current-carrying brass bar, as shown in Fig. 9g.

Tubular samples provide another challenging geometry which can be examined with a variety of different SQUID techniques[39,41]. We have developed a lead-field algorithm to calculate the current distribution from the magnetic field produced by a flaw in a thin-walled, current-carrying cylindrical tube[41,28], and demonstrate in Fig. 17 that the inverse image is consistent with the theoretical prediction.

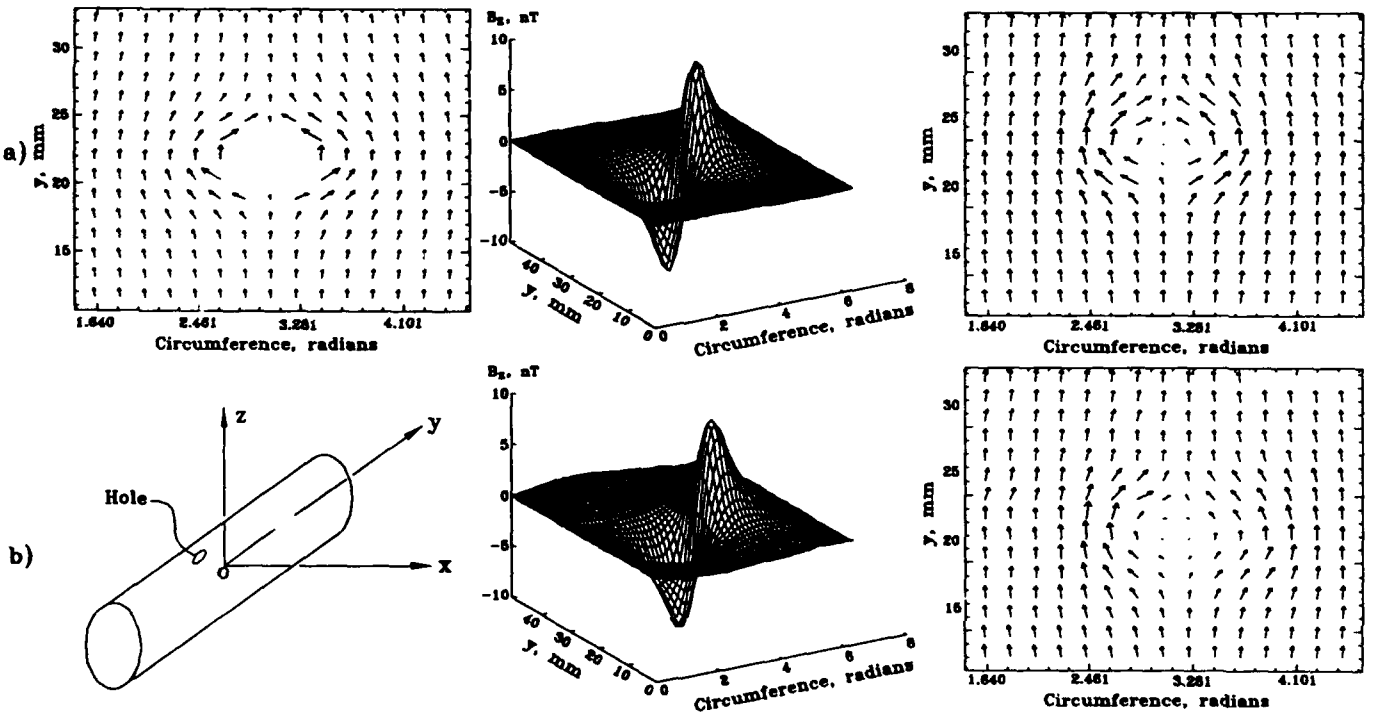

Figure 17. Theoretical and experimental images of current disturbed by a flaw in a thin-walled tube. a) The simulated distribution of current in a thin-walled conducting tube containing a through-wall hole (left) was used to determine the radial component of the magnetic field outside the tube (middle), and a lead field model was used to reconstruct the distribution of current in the tube (right). b) The experimental geometry (left), the measured magnetic field (middle), and the image reconstructed from the data (right). Adapted from Ref. 28.

3. THE FUTURE OF SQUID NDE

3.1 The direction of SQUID NDE research

There are several key issues that need to be addressed in SQUID NDE. SQUID NDE is far from a mature field: there is a vast amount of work between the present, preliminary studies, and a polished, commercial NDE system suitable for use on the flight line. The work can be divided into at least three categories: instrumentation, data acquisition techniques and procedures, and image processing.

3.1.1 Instrumentation. In all likelihood, the instrumentation for SQUID NDE will undergo rapid development in the next several years. Already, compact special-purpose instruments are being fabricated for use in industrial environments[17]. General purpose instruments presently under development will allow the recording of susceptibility images that were impossible just a year or two ago. The future promises to provide fully-integrated digital SQUID magnetometers, with self-contained digital feed-back circuitry, that can be multiplexed within the cryogenic system and would require only minimal room-temperature electronics[18]. Such SQUIDs will be ideally suited for imaging arrays, since an entire array would only require approximately the same number of leads as is presently associated with each analog SQUID channel. Smaller SQUIDs will provide even higher resolution images[52], although some of this resolution will be lost if the sample cannot be cooled to the same temperature as the SQUID. Gradiometers can be optimized for specific measurements[53,54,55] and can be configured in a way to achieve the maximum possible resolution after deconvolution to minimize the effects of a finite-diameter pickup coil[56]. Possibly the greatest short-term improvement will come not with isolated improvements to the SQUID sensors or the cryogenics, but with the creation of optimized systems for which the software and hardware serve as a seamless and essentially invisible interface between the flaw and the operator searching for it. Comparison of today's laboratory SQUID systems with commercial eddy current and ultrasound systems for use on the flight line or on the oil pipeline should provide guidance as to just how important the human factor is in the operation of the instrument.

3.1.2 Data acquisition techniques and procedures. One of the difficulties with SQUID NDE is the sensitivity of the system to fields from irregularities and discontinuities in the sample other than those associated with the flaw. The cancellation approach described above can successfully reduce the signal due to the edge of the plate; immersing an object in a solution whose magnetic susceptibility matches that of the object can eliminate the susceptibility signal from the boundary of an object. Multiple lock-in amplifiers operating at different frequencies can provide images with different sensitivities at different depths, and it may also be possible to use an eddy current approach to reconstruct the current distribution as a function of depth[57]. Tomographic approaches can be used to reconstruct flaws by applying current from differing directions. Matched filters can optimize signals from expected flaws while minimizing the signal from known inhomogeneities characteristic to the sample. Obviously, other approaches will be developed as experience is gained in SQUID NDE. However, in assessing the capabilities of this technique, and comparing it to other approaches, it is important to realize that improved techniques will be developed not only for SQUID NDE but also other NDE methods. The hope for those developing SQUID NDE is that the use of SQUIDs is sufficiently new that there are more improvements to be devised for SQUID NDE than for other techniques!

3.1.3 Image processing. As we discussed above, two of the factors previously limiting the application of SQUID magnetometers to the nondestructive testing of materials and structures have been the lack of sufficient spatial resolution and techniques to provide images of flaws. In the past several years, SQUID NDE has made great progress in overcoming these limitations. However, due to the physical configuration of SQUID magnetometers that measure the field from warm samples, there is an inherent limitation in SQUID spatial resolution capability. In addition, as with any real world measurement procedure, the SQUID measurement process introduces other forms of imaging distortion. In order to remove this distortion and to increase resolution, it is possible to apply the concept of *signal restoration* to the measured images. The objective of a signal restoration algorithm is to reconstruct (or recover) an image from a degraded measure of that image by employing *a priori* knowledge of the distortion process. A critical step in any useful signal restoration algorithm is that of generating a reliable model of the measurement distortion

process. A restored image can be obtained in principal by applying an inverse of this distortion model to the measured image. Our comparisons between numerical models and experimental data suggest that SQUID NDE has the great advantage of providing reproducible, quantitative data well suited for image restoration and quantification of flaw size. The challenge is to optimize the analysis and flaw identification process.

Many of the earlier forms of image restoration were carried out in the spatial frequency domain[27], as was done for Fig. 2. The two-dimensional Fourier transform normally played an important role in such restoration algorithms. However, Fourier-transform-based techniques have an inherent resolution limitation which may limit their use in applications requiring high resolution. Furthermore, it is difficult to apply *a priori* constraints to the image, such as the requirement that no current extend beyond the known borders of the sample. It is for this reason that the spatial domain became the natural terrain for many of the more recently developed image restoration algorithms. In a spatial domain approach, as in the finite element reconstruction shown in Fig. 3, the need to properly model the distortion process remains an essential ingredient. A typical spatial-domain-based image restoration algorithm is heavily based on modern linear algebraic techniques, and possesses the ability to effect "super resolution" image restorations[58]. Undoubtedly, there will be trade-offs dictated by measurement noise, but it is reasonable to assume that such advanced algorithms will be able to provide noticeable enhancement of the images over what we have shown so far.

3.2 SQUID NDE versus other techniques

The second key concern is to further our understanding of the capabilities and limitations of the technique relative to other NDE techniques. This will require detailed, quantitative comparisons of results obtained on a common set of samples. Such an analysis of SQUID NDE could be aided by a theoretical analysis of the sensitivity of a SQUID to a particular type of flaw measured in a certain manner. The development of numerical measurement models that include not only SQUID noise, but also environmental noise and realistic sample inhomogeneities and geometries will prove to be challenging, but will provide a valuable estimate of the smallest flaw that could be detected and the largest flaw that might be missed. The actual determination of a probability of detection (POD) for SQUID NDE of a given class of flaws will require a substantial experimental effort. Although one can always hope to identify a particular flaw that can be detected with SQUIDs and not by any other competing technique, the general acceptance of SQUIDs as regular tools for aircraft NDE will more likely be contingent on whether such a careful POD analysis proves SQUID NDE to be better than competing techniques, at least for a subset of known aircraft flaws.

If it can be shown in the laboratory that SQUIDs have a potential role to play in aircraft NDE, we must then address the constraints imposed by the cryogenic requirements and cost of SQUID systems. At present, SQUIDs are harder to use than eddy current techniques: the probes are larger, heavier, and require scanning systems. They are exquisitely sensitive to magnetic noise from DC to radio frequencies. The systems are presently expensive, costing between $25,000 and $500,000 each, depending upon the complexity and capabilities of the system. SQUID NDE systems are presently comparable in cost and size to ultrasound C-scan systems with water baths and X-ray tomography units. The use of liquid helium, while of little concern to a physicist in a research laboratory, might prove to be an impediment to use of the instrument at an Air Force Air Logistic Center or a commercial airline maintenance depot. The interpretation of the data at present requires sophisticated mathematical models. These are not, however, insurmountable problems, but instead challenges to the clever systems engineer. With the advent of high transition-temperature superconductivity (HTS), SQUIDs and their simplified cryogenic apparatus will quickly become smaller, lighter, and less expensive. Because of the large amplitude of many NDE signals, the somewhat lower sensitivity of HTS SQUIDs as compared to helium-temperature ones is not a major issue. Multiple channel SQUIDs, gradiometers designed to detect flaws but not background signals, and user-friendly electronics might eventually make SQUIDs as easy to use as the Magneto-Optical Inspection technique, but vastly more sensitive. It is also important to recognize that, in contrast with established NDE technologies, the present cost of SQUID systems does not reflect any economies of scale, since most systems sold so far have been custom-built units.

While general-purpose SQUID systems might be useful, the tradeoffs of cost, reliability, and ease of use suggest that the special-purpose SQUID optimized for a single type of flaw and a particular measurement may lead to more rapid introduction of SQUIDs onto the flight line. In that case, we need to identify the type of flaw for which the early flight-line prototypes should be developed.

Unfortunately, once the technical, cost, and practical limitations of SQUIDs are overcome, the acceptance of this technology by the aircraft user and maintenance communities is not guaranteed. The aircraft community is historically conservative with regard to NDE technologies, driven in part by concerns that the premature adoption of a new technology might lead to litigation should an undetected flaw contribute to an accident. If, however, a SQUID NDE system can be developed that is simple to use, inexpensive, is possibly optimized for a single type of flaw, and can detect that type of flaw with unprecedented sensitivity and reliability, then the acceptance of SQUID NDE will be much more likely.

3.3 Promising applications

Given what we have already learned and the expected improvements in SQUID NDE instrumentation and techniques, it is reasonable to hypothesize as to the areas in which SQUID NDE might have the greatest impact. At present we see several, including second-layer cracks and corrosion in aluminum fuselage and wing coverings and susceptibility imaging of composites and magnetic decorants.

3.3.1 Second layer cracks and corrosion. The preliminary data presented above supports our hypothesis that low-frequency eddy-current NDE with SQUIDs is well suited for detecting second-layer cracks. Other techniques have sufficient limitations to justify much more research in this area: ultrasound is capable of detecting flaws in second and third layers only if there is an intact layer of bonding material between each layer; thermography is well suited for detecting disbonds between these layers, but not cracks at rivets; the MOI system cannot at present operate at low enough frequencies to see deep into metallic structures.

3.3.2 Measurements of active corrosion. SQUID magnetometry has seen little application to the study of active corrosion in metals, primarily because of the low spatial resolution provided by SQUIDs optimized for biomagnetic measurements and the unfamiliarity of corrosion scientists with SQUIDs. The most definitive SQUID study to date of corrosion was performed by Bellingham[59], and demonstrated the ability of a low-resolution SQUID to map corrosion currents in a dish. More substantive measurements utilized the SQUID magnetometer solely as a low-impedance ammeter and examined the factors that affected amplitude and spectrum of corrosion noise in a zinc-hydrochloric acid nonvoltaic cell. These particular measurements might have been made more easily using a low impedance, low noise current-to-voltage converter[60]. High resolution studies of corrosion might be facilitated by the use of a high-resolution SQUID magnetometer, such as MicroSQUID[20] or the system recently manufactured by Quantum Magnetics[61].

The ability of SQUID magnetometers to detect steady magnetic fields makes them ideal for mapping of internal corrosion currents. Mathematical models developed by the Vanderbilt group to describe current flow in anisotropic cardiac tissue[62,63] are in fact applicable to the distribution of currents in advanced metallic composite conductors. With a high resolution SQUID such as MicroSQUID, it would be possible to scan an otherwise non-magnetic composite sample of either regular or irregular shape, to determine whether steady magnetic fields are produced by corrosion. A casual experiment at Vanderbilt demonstrated that MicroSQUID was able to detect large DC fields produced by two moistened layers of aluminum spanned by two dissimilar metal rivets. The studies by Bellingham and MacVicar[64] indicate that SQUID magnetometers also have the adequate sensitivity and spatial resolution to measure the frequency spectrum of corrosion currents that arise between a metal and a strong electrolyte; a preliminary study at Vanderbilt demonstrates that MicroSQUID can image the even weaker Johnson noise arising from thermal motion of electrons in a ring of copper. While it is unlikely that Johnson noise images, such as that shown in Fig. 18, will be of practical utility for flight line NDE inspections, these data clearly demonstrate that SQUIDs have adequate sensi-

tivity, spatial resolution, and frequency response to image both the DC component and the full AC spectrum of currents from ongoing corrosion.

Because the magnetic fields from such corrosion currents are weak compared with the earth's magnetic field, and may be subject to contamination by thermoelectric currents in entire aircraft structures, it is likely that SQUID techniques might never be useful for measuring corrosion currents on the flight line. However, this technique provides a new and potentially powerful tool for studying corrosion of aircraft samples in the laboratory. The ability to measure the strength and spatial distribution of filiform currents beneath a layer of paint, and corrosion currents from nonvisible corrosion between the first and second or second and third layers of a sample would provide a new, noninvasive monitoring technique for evaluating the effectiveness of corrosion prevention strategies and for monitoring corrosion development in both time and space.

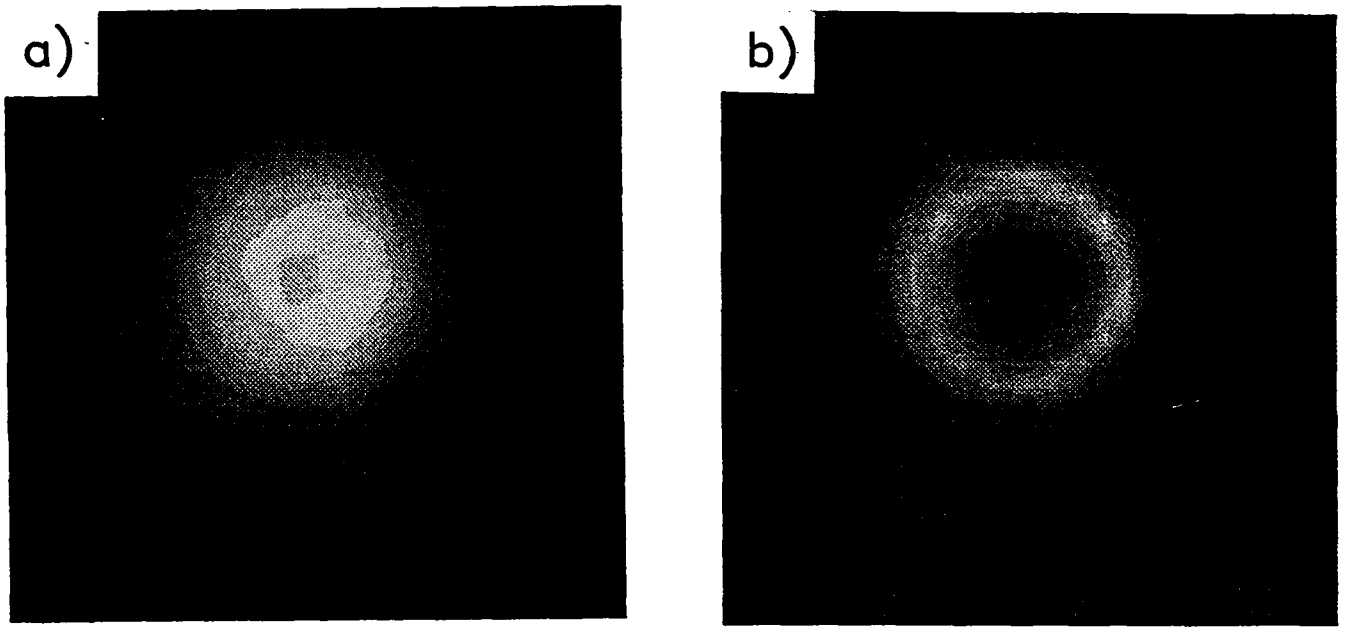

Figure 18. Images of Johnson Noise. Images of the magnetic field produced by Johnson noise currents flowing in a copper ring. a) Images for the 0 to 6 Hz band. b) Images for the 4994 to 5000 Hz band. Note from the magnetic field distribution that the low frequency currents flow around the ring but the high frequency ones only flow locally.

3.3.3 Susceptibility Imaging. The ability of magnetic susceptibility tomography to distinguish materials on the basis of the diamagnetic and paramagnetic susceptibilities may allow for discrimination of materials based upon their chemical makeup. For example, the magnetic susceptibility of aluminum is $+20.9 \times 10^{-6}$ (SI/m^3), while that of aluminum oxide is -18.1×10^{-6}, producing a susceptibility contrast four times greater than the readily imaged susceptibility of plexiglas. For planar samples, scanning susceptometry would provide a real-time 2-D susceptibility image. For three-dimensional objects, susceptibility tomography should be able to identify corrosion products deep inside the sample. The ability to image small quantities of ferromagnetic or superparamagnetic tracers offers promise for rapid detection of surface-breaking flaws in ceramic and other non-metallic materials, as well as in non-ferromagnetic metals. Since MicroSQUID with room-temperature magnetizing coils does not represent an optimized imaging susceptometer, the development of this technique will require a totally-superconducting susceptometer. The increased sensitivity of such a system should provide previously unimagined capabilities for SQUID NDE.

The future of SQUID NDE for aircraft is still uncertain, largely because there have yet to be any proven applications for which SQUID NDE is clearly better than competing techniques. But judging from the progress that has been made in the past several years and the potential for further improvements, SQUID NDE may make its appearance on the flight line within the next few years. The extent to which SQUID NDE can make real inroads into the conventional NDE market will depend in part on the success of the ongoing, initial attempts at transferring this technology out of the laboratory. The research reviewed in this paper should provide some insights as to the direction the field has been taking, and a rather speculative view of the future. All in all, the future of SQUID NDE for aircraft seems bright, but there is much work to be done before this can be assured.

4. ACKNOWLEDGEMENTS

The aircraft NDE research described in this report has been funded primarily by the Air Force Office of Scientific Research, with modest support from Lockheed. The construction of the High Resolution Magnetic Imaging Facility was supported by the AFOSR, the Electric Power Research Institute, the National Institutes of Health, and DuPont. The magnetic susceptibility measurements were funded entirely by DuPont, but are included in this report because of their relevance to future NDE research on non-metallic composites used in advanced aerostructures. The measurements on the tubular samples were supported in part by General Electric.

5. REFERENCES

1. H. Weinstock and M. Nisenoff, "Non-destructive evaluation of metallic structures using a SQUID gradiometer," in *SQUID '85*, Proc. 3rd International Conference on Superconducting Quantum Devices, H.D. Hahlbohm and H. Lubbig, Eds., pp. 843-847, de Gruyter, Berlin, 1985.

2. R.J.P. Bain, G.B. Donaldson, S. Evanson, and G. Hayward, "SQUID gradiometric detection of defects in ferromagnetic structures," in *SQUID '85*, H.D. Hahlbohm and H. Lubbig, Eds., pp. 841-846, de Gruyter, Berlin, 1985.

3. R.J.P. Bain, G.B. Donaldson, S. Evanson, and G. Hayward, "Design and operation of SQUID-based planar gradiometers for non-destructive testing of ferromagnetic plates," *IEEE Trans. on Magnetics*, Vol. Mag-23, pp. 473-476, 1987.

4. A. Cochran and G.B. Donaldson, "Improved techniques for structural NDT using SQUIDs," *NDE Review*, International Superconducting Electronics Conference, Glasgow, 1991.

5. R.B. Mignogna and H.H. Chaskelis, "Investigation of deformation using SQUID magnetometry," Rev. of Progress in QNDE, D.O. Thompson and D.E. Chimenti, Eds., Vol. 8a, pp. 551-558, Plenum, NY, 1989.

6. P. Czipott and W. Podney, "Use of a superconducting gradiometer in an ultrasensitive electromagnetic metal detector," *IEEE Trans. Mag.*, Vol. 25, pp. 1204-1218, 1989.

7. R.L. Fagaly, "SQUID detection of electronic circuits," *IEEE Trans. Mag.*, Vol. 25, pp. 1216-1218, 1989.

8. J.E. Moulder and T.E. Capobianco, "Detection and sizing of surface flaws with a SQUID-based eddy-current probe," *J. Res. Nat. Bureau of Standards*, Vol. 92, pp. 27-33, 1987.

9. J.C. Murphy, G. Hartong, R.F. Cohn, P.J. Moran, K. Bundy, and J.R. Scully, "Magnetic field measurement of corrosion processes," *J. Electrochem. Soc.*, Vol. 135, pp. 310-313, 1988.

10. J.C. Murphy, R. Srinivasan, and R.S. Lillard, "Magnetometer-based measurements of stray current distribution on cathodically protected gas transmission pipeline," Rev. of Progress in QNDE, D.O. Thompson and D.E. Chimenti, Eds., Vol. 8B, pp. 2149-2156, Plenum, NY, 1989.

11. H. Weinstock, T. Erber, and M. Nisenoff, "SQUID detection of Barkhausen threshold and magnetic kaiser effect," A. Schmid, et al., Eds., pp. 935-936, Elsevier Science Publishers, B.V., 1984.

12. H. Weinstock, T. Erber, and M. Nisenoff, "Threshold of Barkhausen emission and onset of hysteresis in iron," *Phys. Rev. B*, Vol. 31, pp. 1535-1553, 1985.

13. R. Srinivasan, J.C. Murphy, C.B. Schroebel, and R.S. Lillard, "Corrosion detection on underground gas pipeline by magnetically assisted ac impedance," *Corrosion '90*, No. 406, 1990.

14. G.B Donaldson, "SQUIDs for everything else," Superconducting Electronics, H. Weinstock and M. Nisenoff, Eds., pp. 175-207, Springer Verlag, NY, 1989.

15. H. Weinstock, "A review of SQUID magnetometry applied to nondestructive evaluation," *IEEE Trans. on Magnetics*, Vol. 27(2), pp. 3231-3236, 1991.

16. 2-G Associates, Mountain View, CA.

17. Tristan Technologies, San Diego, CA.

18. Hypres, Elmsford, NY.

19. Conductus, Mountain View, CA.

20. D.S. Buchanan, D.B. Crum, D. Cox, and J.P. Wikswo, Jr., "MicroSQUID: A close-spaced four channel magnetometer," Adv. in Biomagnetism, S.J. Williamson, G. Hoke, G. Stroink, and M. Kotani, Eds., pp. 677-679, Plenum, NY, 1990.

21. PRI International, Torrance, CA.

22. D.J. Staton, R.N. Friedman, and J.P. Wikswo, Jr., "High resolution SQUID imaging of octupolar currents in anisotropic cardiac tissue," *IEEE Transactions on Applied Superconductivity*, Vol. 3, pp. 1934-1936, 1993.

23. J.P. Wikswo, Jr. and J.M. van Egeraat, "Cellular magnetic fields: Fundamental and applied measurements on nerve axons, Peripheral Nerve Bundles, and Skeletal Muscle," *J. of Clin. Neurophysiology*, Vol. 8, pp. 170-188 1991.

24. Y.P. Ma and J.P. Wikswo, Jr., "A magnetic shield for wide-bandwidth magnetic measurements for non-destructive testing and biomagnetism," *Rev. Sci. Instrum.*, Vol. 62, pp. 2654-2661, 1991.

25. J.P. Wikswo, Jr., J.M. van Egeraat, Y.P. Ma, N.G. Sepulveda, D.J. Staton, S. Tan, and R.S. Wijesinghe, "Instrumentation and techniques for high-resolution magnetic imaging," Digital Image Synthesis and Inverse Optics, A.F. Gmitro, P.S. Idell, and I.J. LaHaie, Eds., Vol. 1351, pp. 438-470, SPIE Proceedings, 1990.

26. D.J. Staton, Y.P. Ma, N.G. Sepulveda, and J.P. Wikswo, Jr., "High-resolution magnetic mapping using a SQUID magnetometer array," *IEEE Trans. on Magnetics*, Vol. MAG-27, pp. 3237-3240, 1991.

27. B.J. Roth, N.G. Sepulveda, and J.P. Wikswo, Jr., "Using a magnetometer to image a two-dimensional current distribution," *J. Appl. Phys.*, Vol. 65, pp. 361-372, 1989.

28. S. Tan, Y.P. Ma, I.M. Thomas, and J.P. Wikswo, Jr., "High resolution SQUID imaging of current and magnetization distributions," *IEEE Transactions on Applied Superconductivity*, Vol. 3, pp. 1945-1948, 1993.

29. Shaofen Tan, "Linear system imaging and its applications to magnetic measurements by SQUID magnetometers," *Ph.D. Dissertation*, Department of Physics and Astronomy, Vanderbilt University, 1992.

30. W. Benzing, T. Scherer, and W. Jutzi, "Inversion calculation of two-dimensional current distributions from their magnetic field," *IEEE Transactions on Applied Superconductivity*, Vol. 3, pp. 1902-1905, 1993.

31. Y.P. Ma, D.J. Staton, N.G. Sepulveda, and J.P. Wikswo, Jr., "Imaging flaws with a SQUID magnetometer array," Rev. of Progress in QNDE, D.O. Thompson and D.E. Chimenti, Eds., Vol. 10A, pp. 979-986, Plenum, New York, 1991.

32. J.P. Wikswo, Jr., D.B. Crum, W.P. Henry, Y.P. Ma, N.G. Sepulveda, and D.J. Staton, "An improved method for magnetic identification and localization of cracks in conductors," *Journal of Nondestructive Evaluation*, Vol. 12(2), in press.

33. Steve Baughman, Lockheed Aeronautical Systems Company of Marietta, GA.

34. Y.P. Ma and J.P. Wikswo, Jr., "Imaging subsurface defects using SQUID magnetometers," Review of Progress in QNDE, D.O. Thompson and D.E. Chimenti, Eds, Vol. 12: pp. 1137-1143, Plenum, New York, 1993.

35. Sample provided by Jan Achenbach, Northwestern University, Evanston, IL.

36. Yu Pei Ma, personal communication.

37. Y.P. Ma and J.P. Wikswo, Jr., "Detection of deep flaw inside a conductor using a SQUID magnetometer," Rev. of Progress in QNDE, D.O. Thompson and D.E. Chimenti, Eds., Vol. 11, pp. 1153-1159, 1992.

38. D.K. Thome, G.L. Fitzpatrick, E.Y.C. Shih, R.L. Skaugset, W.C.L. Shih, "Aircraft inspection with the magneto-optic/eddy current imager: A new technology", Presented at the ATA NDT Forum, Long Beach, CA, 1991.

39. W.C.L. Shih, G.L. Fitzpatrick, D.K. Thome, R.L. Skaugset, E.Y.C. Shih, "Aircraft inspection with the magneto-optic/eddy current imager", Int. Conf. on Surface Treatments in the Aeronautical and Aerospace Industries, Cannes, France, 1992.

40. D.C. Hurley, Y.P. Ma, S. Tan, and J.P. Wikswo, Jr., "A comparison of SQUID imaging techniques for small defects in nonmagnetic tubes," *Review of Progress in QNDE*, Vol. 12, 633-640, 1993.

41. D.C. Hurley, Y.P. Ma, S. Tan, and J.P. Wikswo, Jr., "Imaging of small defects in nonmagnetic tubing using a SQUID magnetometer," *Res. Nondestr. Eval.*, Vol. 5, pp. 1-29, 1993.

42. J.P. Wikswo, Jr., Y.P. Ma, N.G. Sepulveda, S. Tan, I.M. Thomas, and A. Lauder, "Magnetic susceptibility imaging for nondestructive evaluation," *IEEE Transactions on Applied Superconductivity*, Vol. 3, pp. 1995-2002, 1993.

43. Y.P. Ma, I.M. Thomas, A. Lauder, and J.P. Wikswo, Jr., "A high resolution imaging susceptometer," *IEEE Transactions on Applied Superconductivity*, Vol. 3, pp. 1941-1944, 1993.

44. I.M. Thomas, Y.P. Ma, S. Tan, and J.P. Wikswo, Jr., "Spatial resolution and sensitivity of magnetic susceptibility imaging," *IEEE Transactions on Applied Superconductivity*, Vol. 3, pp. 1937-1940, 1993.

45. I.M. Thomas, Y.P. Ma, and J.P. Wikswo, Jr., "SQUID NDE: Detection of surface flaws by magnetic decoration," *IEEE Transactions on Applied Superconductivity*, Vol. 3, pp. 1949-1952, 1993.

46. I.M. Thomas, T.C. Moyer, and J.P. Wikswo, Jr., "High resolution magnetic susceptibility imaging of geological thin sections: Pilot study of a pyroclastic sample from the Bishop tuff," *Geophysical Research Letters*, Vol. 19(21), pp. 2139-2142, 1992.

47. Y.P. Ma and J.P. Wikswo, Jr., "The magnetic field produced by a elliptical flaw in a current carrying plate," in preparation.

48. N.G. Sepulveda, D.J. Staton, and J.P. Wikswo, Jr., "A mathematical analysis of the magnetic field produced by flaws in two-dimensional current carrying conductors," *J. Nondestructive Evaluation*, Vol. 11, pp. 89-101, 1992.

49. S. Tan, B.J. Roth, and J.P. Wikswo, Jr., "The magnetic field of cortical current sources: The application of a spatial filtering model to the forward and inverse problems," *Electroencephalography and Clinical Neurophysiology*, Vol. 76, pp. 73-85, 1990.

50. Y.P. Ma and J.P. Wikswo, "Mathematical model for the magnetic field of finite-depth cylindrical flaws in thick, current-carrying plates," in preparation.

51. Y.P. Ma and J.P. Wikswo, Jr., "The magnetic field produced by a spherical flaw inside a thick current carrying plate," in preparation.

52. A. Mathai, D. Song, Y. Gin, and F.C. Wellstood, "High resolution magnetic microscopy using a dc SQUID," *IEEE Transactions on Applied Superconductivity*, Vol. 3, 2609-2612, 1993.

53. J.P. Wikswo, Jr., "Optimization of SQUID differential magnetometers," *AIP Conf. Proc.*, Vol. 44, pp. 145-149, 1978.

54. J.P. Wikswo, Jr., "Design considerations for magnetic imaging with SQUID microscopes and arrays," International Superconducting Electronics Conference, Boulder, CO, 1993, in press.

55. J.P. Wikswo, Jr., "High-resolution measurements of biomagnetic fields," *Advances in Cryogenic Engineering*, R.W. Fast, Ed., Vol. 33, pp. 107-116, 1988.

56. B.J. Roth and J.P. Wikswo, Jr., "Apodized pickup coils for improved spatial resolution of SQUID magnetometers," *Review Sci. Instr.*, Vol. 61, pp. 2439-2448, 1990.

57. Y.P. Ma and J.P. Wikswo, Jr., "Improved techniques to induce low frequency eddy currents for SQUID-based non-destructive testing," in preparation.

58. J.A. Cadzow, "Signal enhancement: A composite property algorithm," *IEEE Transactions on Acoustics, Speech, and Signal Processing*, Vol. ASSP 36, pp. 49-62, 1988.

59. J.G. Bellingham, "Magnetic detection and characterization of electrochemical noise processes," *Ph.D. Dissertation*, Department of Physics, MIT, 1988.

60. J.P. Wikswo, Jr., P.C. Samson, and R.P. Giffard, "A low-noise, low input impedance amplifier for magnetic measurements of nerve action currents," *IEEE Trans. Biomed. Eng.*, Vol. BME-30, pp. 215-221, 1983.

61. A.D. Hibbs, R.E. Sager, D.W. Cox, T.H. Aukerman, T.A. Sage, and R.S. Landis, "A high-resolution magnetic imaging system based on a SQUID magnetometer," *Rev. Scientific Instruments*, Vol. 63, pp. 3652-3658, 1992.

62. N.G. Sepulveda and J.P. Wikswo, Jr., "Electric and magnetic fields from two-dimensional anisotropic bisyncytia," *Biophysical J.*, Vol. 51, pp. 557-568, 1987.

63. N.G. Sepulveda, B.J. Roth, and J.P. Wikswo, Jr., "Current injection into a two-dimensional anisotropic bidomain," *Biophysical J.*, Vol. 55, pp. 987-999, 1989.

64. J.G. Bellingham and M.L.A MacVicar, "SQUID technology applied to the study of electrochemical corrosion," *IEEE Trans. Mag.*, Vol. Mag-23, pp. 477-479, 1987.

APPENDIX A

Vanderbilt Electromagnetics Laboratory
High resolution SQUID Magnetometry for Non-destructive Evaluation

Project Publications

Journal Articles:

1. "Using a Magnetometer to Image a Two-dimensional Current Distribution," B.J. Roth, N.G. Sepulveda, and J.P. Wikswo, Jr., J. Appl. Phys., 65: 361-372 (1989).

2. "Apodized Pickup Coils for Improved Spatial Resolution of SQUID Magnetometers," B.J. Roth and J.P. Wikswo, Jr., Review Sci. Instr., 61: 2439-2448 (1990).

3. "A Magnetic Shield for Wide-Bandwidth Magnetic Measurements for Non-Destructive Testing and Biomagnetism," Y.P. Ma and J.P. Wikswo, Jr., Rev. Sci. Instrum., 62(11): 2654-2661 (1991).

4. "A Mathematical Analysis of the Magnetic Field Produced By Flaws in Two-Dimensional Current-Carrying Conductors," N.G. Sepulveda, D.J. Staton and J.P. Wikswo, Jr., Journal of Nondestructive Evaluation, 11(2): 89-101 (1992).

5. "An Improved Method for Magnetic Identification and Localization of Cracks in Conductors," J.P. Wikswo, Jr., D.B. Crum, W.P. Henry, Y.P. Ma, N.G. Sepulveda, and D.J. Staton, Journal of Nondestructive Evaluation, 12(2): in press.

6. "Imaging of Small Defects in Nonmagnetic Tubing Using a SQUID Magnetometer," D.C. Hurley, Y.P. Ma, S. Tan, and J.P. Wikswo, Jr., Research in Nondestructive Evaluation, in press.

Patents:

1. "A Magnetometer Flux Pick-up Coil with Non-uniform Interturn Spacing Optimized for Spatial Resolution," B.J. Roth and J.P. Wikswo, Jr., United States Patent, 5,038,104 (August 6, 1991).

2. "Method and Apparatus for Magnetic Identification and Localization of Flaws in Conductors by Cancelling the Field About the Conductor with the Field about a Flawless Conductor, J.P. Wikswo, Jr., D.B. Crum, W.P. Henry, and N.G. Sepulveda, United States Patent, 5,109,196 (April 29, 1992).

Manuscripts in Preparation:

1. "Optimization of High-Resolution SQUID Magnetometers with Rectangular Pickup Coils," R.S. Wijesinghe and J.P. Wikswo, Jr.

2. "The Magnetic Field Produced by a Cylindrical Flaw with Finite Depth in a Thick Current Carrying Plate," Y.P. Ma and J.P. Wikswo, Jr.

3. "The Magnetic Field Produced by a Elliptical Flaw in a Current Carrying Plate," Y.P. Ma and J.P. Wikswo, Jr.

4. "The Magnetic Field Produced by a Spherical Flaw Inside a Thick Current Carrying Plate," Y.P. Ma and J.P. Wikswo, Jr.

5. "Improved Techniques for Inducing Low Frequency Eddy Currents for SQUID-Based Non-Destructive Testing," Y.P. Ma and J.P. Wikswo, Jr.

6. "The Spatial Distributions of Magnetization and Transport Current in $Tl_2Ca_1Ba_2Cu_2O_8$ Polycrystalline Superconducting Thin Films," S. Tan, Y.P. Ma, and J.P. Wikswo, Jr.

7. "A Comparison of the V_3 Transformation and the Exact Algorithm for Magnetic Imaging of Current Distributions," S. Tan and J.P. Wikswo, Jr.

Conference Proceedings:

1. "MicroSQUID: A Close-Spaced Four Channel Magnetometer," D.S. Buchanan, D.B. Crum, D. Cox, and J.P. Wikswo, Jr., Advances in Biomagnetism, S.J. Williamson, M. Hoke, G. Stroink, and M. Kotani, Eds., (Plenum, New York), pp. 677-679 (1990).

2. "Instrumentation and Techniques for High-Resolution Magnetic Imaging," J.P. Wikswo, Jr., J.M. van Egeraat, Y.P. Ma, N.G. Sepulveda, D.J. Staton, S. Tan, and R.S. Wijesinghe, Digital Image Synthesis and Inverse Optics, A.F. Gmitro, P.S. Idell, and I.J. LaHaie, Eds., SPIE Proceedings, Vol. 1351, pp. 438-470 (1990).

3. "Imaging Flaws with a SQUID Magnetometer Array," Y.P. Ma, D.J. Staton, N.G. Sepulveda, and J.P. Wikswo, Jr., Rev. of Progress in Quantitative Nondestructive Evaluation, D.O. Thompson and D.E. Chimenti, Eds., (Plenum, New York), Vol. 10A, pp. 979-986 (1991).

4. "High-Resolution Magnetic Mapping Using a SQUID Magnetometer Array," D.J. Staton, Y.P. Ma, N.G. Sepulveda, and J.P. Wikswo, Jr., IEEE Trans. on Magnetics, MAG-27(2): 3237-3240 (1991).

5. "Detection of Deep Flaw Inside a Conductor Using a SQUID Magnetometer," Y.P. Ma and J.P. Wikswo, Jr., Review of Progress in QNDE, 11: 1153-1159 (1992).

6. "High Resolution SQUID Imaging of Current and Magnetization Distribution," S. Tan, Y.P. Ma, I.M. Thomas, and J.P. Wikswo, Jr., IEEE Transactions on Applied Superconductivity, 3(1): 1945-1948 (1993).

7. "A Comparison of SQUID Imaging Techniques for Small Defects in Nonmagnetic Tubes," D.C. Hurley, Y.P. Ma, S. Tan, and J.P. Wikswo, Jr., Review of Progress in QNDE, 12: 633-640 (1993).

8. "Imaging Subsurface Defects Using SQUID Magnetometers," Y.P. Ma and J.P. Wikswo, Jr., Review of Progress in QNDE, 12: 1137-1143 (1993).

9. "Detection of Subsurface Flaws Using SQUID Eddy Current Technique," Yu Pei Ma and John P. Wikswo, Jr., Society of Photo-Optical Instrumentation Engineers, San Diego, CA, 1993, (in press).

10. "Superconducting Magnetometry: A Possible Technique for Aircraft NDE," J.P. Wikswo, Jr., Y.P. Ma, N.G. Sepulveda, D.J. Staton, S. Tan, and I.M. Thomas, Society of Photo-Optical Instrumentation Engineers, San Diego, CA, 1993, (in press).

11. "Design Considerations For Magnetic Imaging with SQUID Microscopes and Arrays," J.P. Wikswo, Jr., International Superconductive Electronics Conference, Boulder, CO, 1993 (in press).

Abstracts:

1. "High-Resolution SQUID Magnetometers for Biophysics and Non-Destructive Testing," J.P. Wikswo, Jr. and B.J. Roth, Bull. Am. Phys. Soc., 32: 2131 (1987).

2. "SQUID Magnetometry for Non-Destructive Testing," J.P. Wikswo, Jr., J. Tenn. Acad. Sci., 63: 51-52 (1988).

3. "The Imaging of Small Current Sources by SQUID Magnetometer," S. Tan and J.P. Wikswo, Jr., J. Tenn. Acad. Sci., 65: 48 (1990).

4. "High-Resolution Magnetic Mapping using a SQUID Magnetometer Array," D.J. Staton, N.G. Sepulveda, and J.P. Wikswo, Jr., Bull. Am. Phys. Soc., 35: 2367 (1990).

Ph.D. Degrees Supervised:

5. Shaofen Tan, "Linear System Imaging and its Applications to Magnetic Measurements by SQUID Magnetometers," Ph.D., 1992.